

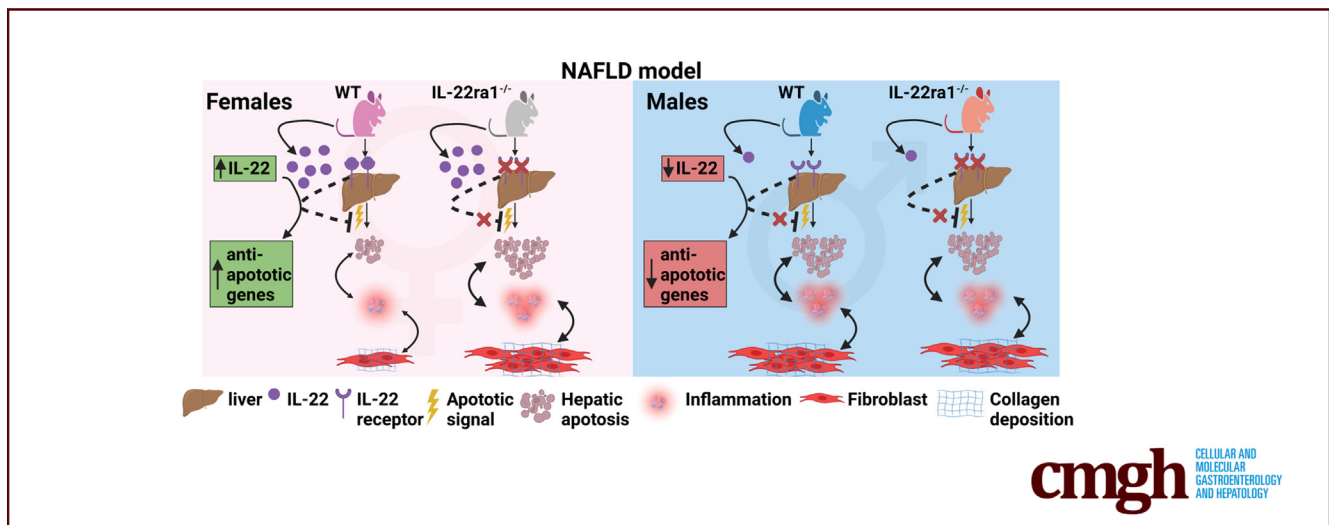
ORIGINAL RESEARCH

Sex-Dependent Hepatoprotective Role of IL-22 Receptor Signaling in Non-Alcoholic Fatty Liver Disease-Related Fibrosis



Mohamed N. Abdelnabi,^{1,2} Manuel Flores Molina,^{1,2} Geneviève Soucy,^{1,3} Vincent Quoc-Huy Trinh,^{1,3} Nathalie Bédard,^{1,2} Sabrina Mazouz,^{1,2} Nathalie Juvet,⁴ Jessica Dion,^{1,2} Sarah Tran,^{1,2} Marc Bilodeau,^{1,5} Jennifer L. Estall,^{4,5} and Naglaa H. Shoukry^{1,5}

¹Centre de Recherche du Centre Hospitalier de l'Université de Montréal, Montréal, Québec, Canada; ²Département de Microbiologie, Infectiologie et Immunologie, Faculté de Médecine, Université de Montréal, Montréal, Québec, Canada; ³Département de Département de Pathologie et Biologie Cellulaire, Faculté de Médecine, Université de Montréal, Montréal, Québec, Canada; ⁴Institut de Recherches, Cliniques de Montreal, Montréal, Québec, Canada; and ⁵Département de Médecine, Faculté de Médecine, Université de Montréal, Montréal, Québec, Canada



SUMMARY

We report sexual dimorphism in hepatic interleukin 22 expression in human beings and mice with nonalcoholic fatty liver disease (NAFLD). Lack of interleukin 22–receptor signaling exacerbated fibrosis in female, but not male, mice with NAFLD, suggesting a sex-dependent hepatoprotective role of this pathway in NAFLD-related liver injury.

BACKGROUND & AIMS: Nonalcoholic fatty liver disease (NAFLD) is a major health problem with complex pathogenesis. Although sex differences in NAFLD pathogenesis have been reported, the mechanisms underlying such differences remain understudied. Interleukin (IL)22 is a pleiotropic cytokine with both protective and/or pathogenic effects during liver injury. IL22 was shown to be hepatoprotective in NAFLD-related liver injury. However, these studies relied primarily on exogenous administration of IL22 and did not examine the sex-dependent effect of IL22. Here, we sought to characterize the role of endogenous IL22-receptor signaling during NAFLD-induced liver injury in males and females.

METHODS: We used immunofluorescence, flow cytometry, histopathologic assessment, and gene expression analysis to examine IL22 production and characterize the intrahepatic immune landscape in human subjects with NAFLD (n = 20; 11 men and 9 women) and in an *in vivo* Western high-fat diet–induced NAFLD model in IL22RA knock out mice and their wild-type littermates.

RESULTS: Examination of publicly available data sets from 2 cohorts with NAFLD showed increased hepatic IL22 gene expression in females compared with males. Furthermore, our immunofluorescence analysis of liver sections from NAFLD subjects (n = 20) showed increased infiltration of IL22-producing cells in females. Similarly, IL22-producing cells were increased in wild-type female mice with NAFLD and the hepatic IL22/IL22 binding protein messenger RNA ratio correlated with expression of anti-apoptosis genes. The lack of endogenous IL22-receptor signaling (IL22RA knockout) led to exacerbated liver damage, inflammation, apoptosis, and liver fibrosis in female, but not male, mice with NAFLD.

CONCLUSIONS: Our data suggest a sex-dependent hepatoprotective antiapoptotic effect of IL22-receptor signaling during NAFLD-related liver injury in females. (*Cell Mol*

Gastroenterol Hepatol 2022;14:1269–1294; <https://doi.org/10.1016/j.jcmgh.2022.08.001>

Keywords: NAFLD; liver fibrosis; IL22 receptor signaling; IL22BP.

Nonalcoholic fatty liver disease (NAFLD) has become the most prevalent chronic liver disease as a result of the increase in obesity, insulin resistance (IR), and type 2 diabetes mellitus.^{1,2} Although, the prevalence of NAFLD seems to be higher in males than in females, this sex difference likely is inconclusive and could be cofounded by age.^{3,4} Sex differences in NAFLD pathogenesis are reported but the underlying mechanisms remain understudied.^{4–6} NAFLD spans a wide spectrum of liver disease ranging from hepatic steatosis, nonalcoholic steatohepatitis (NASH), advanced fibrosis, cirrhosis, and, ultimately, hepatocellular carcinoma.^{7,8} NASH-induced inflammation can enhance activation of hepatic stellate cells (HSCs), thus accelerating fibrosis progression.^{7,9} Importantly, liver-related mortality increases exponentially with the increase in fibrosis stage in patients with NAFLD.¹⁰ Currently, there are no approved therapies for NASH, but many interventional studies are ongoing.^{7,8}

Interleukin (IL)22 is a pleiotropic cytokine with both inflammatory and protective effects during injury and repair in various tissues including the liver.¹¹ IL22 is a member of the IL10 cytokine family and is produced by multiple immune cells including helper T cell (Th)17, Th22, Tc22, and $\gamma\delta$ -T cells, natural killer (NK) cells, innate lymphoid cells 3 (ILC3s), macrophages, and neutrophils.^{11–14} The IL22 receptor (IL22R) is composed of 2 subunits: IL22RA1 and IL10RB2.^{11,15} The IL10RB2 subunit is expressed constitutively throughout the body, but expression of the IL22RA1 subunit is limited mainly to epithelial cells and some fibroblasts.^{11,16,17} Thus, although IL22 is produced by many immune cells, its effect(s) is restricted mainly to epithelial cells.^{11,16}


IL22 was reported to be hepatoprotective in various models of liver injury.^{18–22} This effect is mediated by enhancing signal transducer and activator of transcription 3 (STAT-3) downstream signaling, including induction of the anti-apoptotic proteins (B-cell lymphoma 2 [BCL] and BCL-extra large), mitogenic proteins (c-mycelocytomatosis protein and cyclin D1), and antioxidant proteins (metallothionein [MT]2), leading to prevention of hepatocyte death and enhancing hepatocyte proliferation.^{18–22} IL22 also induces intrinsic antimicrobial activity in the liver through increased expression of antimicrobial peptides such as lipocalin 2 and serum amyloid A 2.²³ Furthermore, IL22 promotes liver regeneration, and was reported to induce senescence of activated HSCs and thus reduce liver fibrosis progression.^{24–26} Finally, emerging evidence has identified IL22 as a mitochondrial protector against liver injury.²⁷ A recombinant fusion protein of human IL22 dimer (IL-22Fc) was safe in phase 1 clinical trials,^{28,29} and decreased inflammatory markers along with amelioration in model for end-stage liver disease scores in a phase 2 trial in alcoholic steatohepatitis.³⁰

IL22 also may be proinflammatory during hepatitis B virus infection and in hepatitis B virus transgenic mouse models.^{31,32} We and others have shown that IL22-producing cells were enriched significantly in liver tissue samples with advanced fibrosis, in particular, in patients with viral hepatitis, suggesting a profibrogenic role of IL22 during chronic liver injury.^{33,34} Furthermore, we validated this finding *in vivo* in the carbon tetrachloride (CCl₄)- and thioacetamide-induced chronic liver injury models, in which a lack of endogenous IL22 signaling in IL22RA1 knockout (IL22ra1^{-/-}) mice led to reduced hepatic fibrosis.³³ In contrast, other studies have reported that exogenous IL22 administration in the chronic CCl₄ model was hepatoprotective and resulted in fibrosis resolution.^{24,25} The profibrogenic role of IL22 also was documented in other organs such as the pancreas.³⁵ These different observations highlight the dual nature of IL22 that likely is dictated by multiple factors including the tissue involved, pathologic environment, endogenous vs exogenous IL22 level, and the time of exposure.^{24,25,32,33,36}

IL22 activity is regulated by the IL22 binding protein (IL22BP or IL22RA2), which is a soluble decoy IL22 receptor that acts as an endogenous high-affinity inhibitor of IL22.^{11,15} Indeed, a proinflammatory role of IL22 has been observed in ischemia-reperfusion and acetaminophen-induced liver injury models using IL22BP-deficient mice (IL22BP^{-/-}).³⁷ The lack of IL22BP in these models resulted in uncontrolled regulation of IL22 signaling and exacerbation of hepatocyte death, which was associated with increased chemokine (C-X-C motif) ligand expression in hepatocytes and promoted infiltration of inflammatory monocytes to the liver.³⁷ In contrast, another study in subjects chronically infected with *Schistosoma japonicum* reported that IL22 transcripts were increased, while IL22BP transcripts were reduced. This was associated with decreased hepatic fibrosis, suggesting a protective role of IL22 in these subjects.³⁸

Most studies have reported a hepatoprotective role and beneficial metabolic effects of IL22 in NAFLD. IL22 decreased body weight, ameliorated glucose intolerance,

Abbreviations used in this paper: ALT, alanine aminotransferase; BCL, B-cell lymphoma; BP, binding protein; CCl₄, carbon tetrachloride; cDNA, complementary DNA; CHUM, Centre Hospitalier de l'Université de Montréal; CRCHUM, Centre de Recherche du Centre Hospitalier de l'Université de Montréal; HFD, high-fat diet; HSC, hepatic stellate cell; IF, immunofluorescence; IHL, intrahepatic leukocyte; IL, interleukin; ILC3, innate lymphoid cell 3; IL22R, interleukin 22 receptor; IL22ra1^{-/-}, interleukin 22ra knockout; IR, insulin resistance; MPO, myeloperoxidase; mRNA, messenger RNA; MT, metallothionein; NAFLD, nonalcoholic fatty liver disease; NAS, NAFLD activity score; NASH, nonalcoholic steatohepatitis; NK, natural killer; PBS, phosphate-buffered saline; PMA, phorbol myristate acetate; PSR, picrosirius red; qPCR, quantitative polymerase chain reaction; STAT-3, signal transducer and activator of transcription 3; TG, triglyceride; TGF- β , transforming growth factor β ; Th, helper T cell; TUNEL, terminal deoxynucleotidyl transferase-mediated deoxyuridine triphosphate nick-end labeling; WT, wild-type.

 Most current article

© 2022 The Authors. Published by Elsevier Inc. on behalf of the AGA Institute. This is an open access article under the CC BY-NC-ND license (<http://creativecommons.org/licenses/by-nc-nd/4.0/>).

2352-345X

<https://doi.org/10.1016/j.jcmgh.2022.08.001>

improved insulin sensitivity, and reduced adiposity and hepatic triglyceride (TG) levels in various NAFLD models.^{39–42} IL22Fc ameliorated neutrophil-induced oxidative stress via STAT-3-mediated induction of MT1 and MT2 antioxidant proteins and subsequently reduced NASH-related inflammation and fibrosis.²² However, these effects were observed with high levels of exogenously administered IL22 (eg, IL22Fc).²² Studies investigating the role of endogenous IL22 are limited. Rolla et al⁴³ showed that endogenous IL22 produced by Th22 cells antagonized inflammation development and fibrosis progression in a methionine-choline-deficient diet-induced NASH model, but only in the absence of IL17 (IL17^{-/-} mice). However, this model lacks metabolic abnormalities associated with NAFLD and does not completely recapitulate human NASH. Finally, these studies were limited to male mice and thus data regarding the sex-based immunologic difference between males and females in the context of NAFLD remain elusive.

Here, we investigated the role of endogenous IL22-receptor signaling in NAFLD-related liver injury in both males and females using a combination of human samples and an *in vivo* mouse model using IL22ra1^{-/-} mice and their wild-type (WT) littermates. We report that hepatic IL22 expression had sexually dimorphic differences in both human beings and mice with NAFLD, in which it was increased in females vs males. This was associated with an increase in hepatic IL22BP expression in female mice with NAFLD compared with males. In addition, the hepatic IL22/IL22BP messenger RNA (mRNA) ratio correlated positively with IL22 downstream target genes (anti-apoptotic and antioxidant genes) in those females. Lack of endogenous IL22-receptor signaling in female mice with NAFLD, but not males, exacerbated liver injury, inflammation, and fibrosis.

Results

Increased Intrahepatic IL22-Producing Cells in Female Subjects With NAFLD as Compared With Males

To evaluate the endogenous role of IL22 in human subjects with NAFLD, we queried 2 publicly available microarray data sets (GSE106737 and GSE151158) and compared the hepatic IL22 expression between females and males with NAFLD.^{44,45} We detected a marked up-regulation of *IL22* mRNA expression in livers of females compared with males (Figure 1A and B). Next, we conducted immunofluorescence (IF) staining to quantify IL22-producing cells *in situ* in liver biopsy samples from a third cohort of NAFLD patients (n = 20) recruited at our institution (Tables 1 and 2). There was no difference in either the nonalcoholic fatty liver disease activity score (NAS) or the fibrosis scores between female and male subjects (Table 1), indicating that both groups had comparable NAFLD severity profiles. In line with IL22 transcriptomic data, IL22-producing cells were increased significantly ($P = .0002$) in the livers of females compared with males (Figure 1C and E). To identify IL22-producing cells in female subjects with NAFLD, we performed multiplex IF staining of IL22 and either the T-cell marker (CD3⁺) or the neutrophil marker (CD66b⁺).

Surprisingly, CD3⁺ T cells identified *in situ* by IF did not colocalize with IL22 (Figure 1F), while the majority of IL22-producing cells co-expressed CD66b⁺, suggesting that they may be neutrophils (Figure 1G). Nevertheless, the lack of detection of IL22-producing T cells by IF in those females was inconclusive because we could not further characterize IL22-producing cells by other techniques such as flow cytometry because we did not have access to fresh liver biopsy specimens from these subjects. Overall, these results suggest a sexual dimorphic expression of IL22 in the context of NAFLD.

Increased Intrahepatic IL22-Producing Cells in High-Fat Diet-Fed Female Mice as Compared With Males

Next, we sought to validate our observation of sexual dimorphic expression of IL22 in an *in vivo* model of NAFLD. WT C57BL/6N mice, including males and females, were placed on either a high-fat diet (HFD) that simulates Western diet, or a control diet for 30 weeks as described in the Materials and Methods section. To assess the hepatic infiltration of IL22-producing cells, we quantified IL22 cytokine/protein expression *in situ* using IF, and gene expression using quantitative polymerase chain reaction (qPCR). Interestingly, endogenous IL22 expression was increased significantly at both the protein and mRNA levels in livers of WT female mice compared with males ($P < .001$ and $P < .0001$, respectively) after 30 weeks on a HFD (Figure 2A–D). Because IL23 is established as a key inducer of IL22 production by different innate and adaptive immune cells,^{13,46} we examined hepatic *Il23* gene expression. Similar to IL22, we observed substantial up-regulation of *Il23* expression in the livers of HFD-fed WT female mice compared with their male littermates (Figure 2E). To identify the cellular sources of IL22 in HFD-fed WT female mice, we performed multiplex IF staining of IL22 and either the T-cell marker (CD3⁺) or the neutrophil marker (Ly6G⁺). As observed in our human study, CD3⁺ T cells identified *in situ* by IF did not colocalize with IL22 (Figure 2F), but neutrophils (Ly6G⁺ cells) were one of the IL22 cellular sources, although they were not the major source (Figure 2G). To better characterize IL22-producing T cells in our NAFLD model, we extracted the intrahepatic lymphocytes from HFD-fed WT female or male mice and examined their capacity to produce IL22 by flow cytometry after stimulation with phorbol myristate acetate (PMA)/ionomycin. We observed Th17 (IL22⁺ IL17A⁺ CD4⁺), Th22 (IL22⁺ IL17A⁻ CD4⁺), and $\gamma\delta$ -T cells (IL22⁺ CD3⁺ T cell receptor $\gamma\delta$ ⁺) as the major IL22-producing cells, and, to a lesser extent, ILC3s (CD3⁻NKp46⁺) (Figure 3A and D). In addition, the IL22 production by these cells was significantly higher in HFD-fed WT female mice compared with the controls ($P < .05$) (Figure 3C–E). Moreover, the HFD-fed WT female mice showed increased IL22 production by these lymphocyte subsets compared with the same cells in male mice (Figure 3A and B). This further validates the high level of hepatic IL22 observed in female mice by IF and qPCR (Figure 2A, C, and D). Notably, we did not observe a

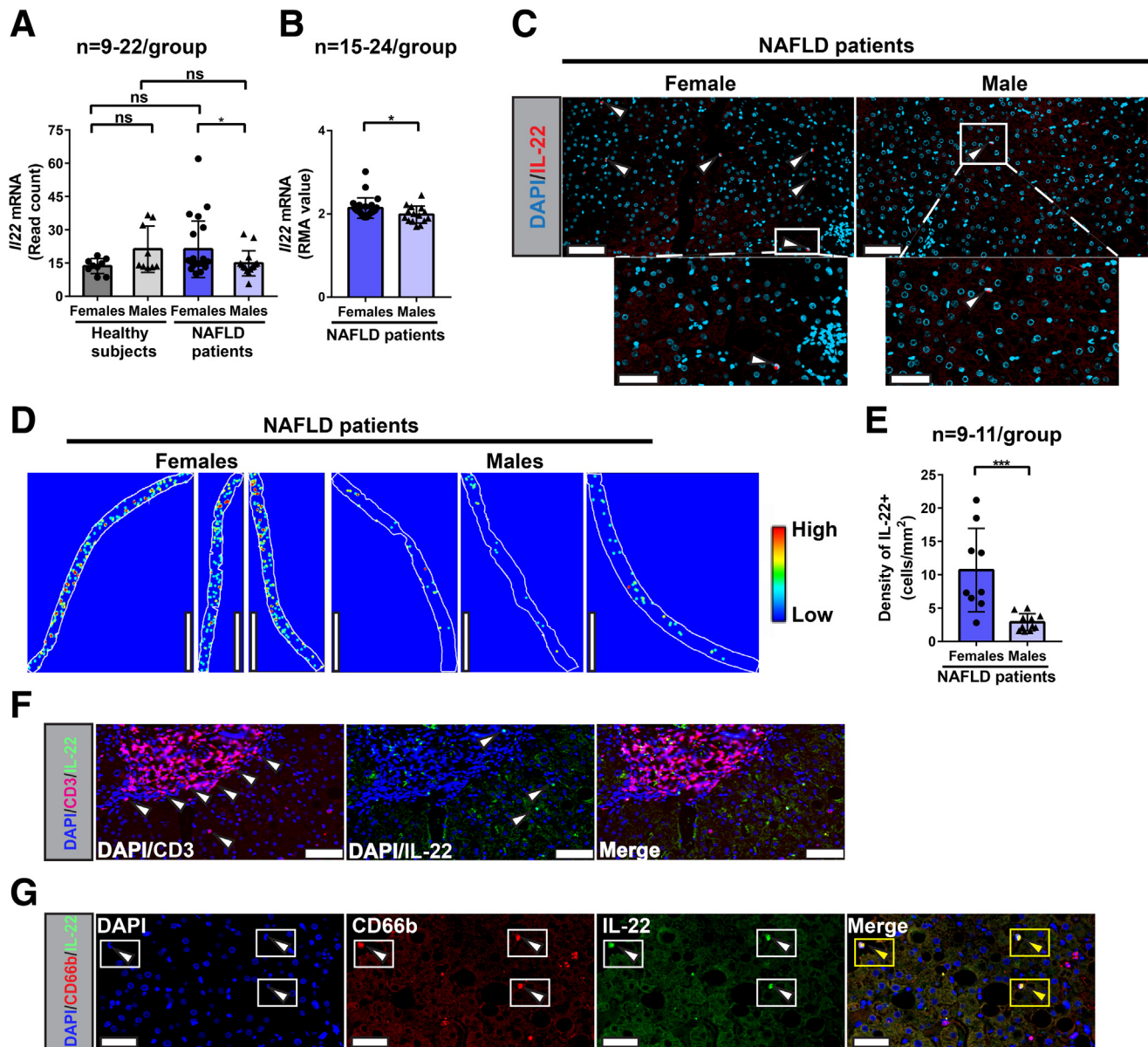


Figure 1. Increased levels of IL22⁺ cells in livers of female vs male patients with NAFLD. (A and B) IL22 mRNA expression from publicly available microarray data sets (GSE151158 and GSE106737) of 2 different cohorts of NAFLD patients. IL22 mRNA levels were normalized and expressed as read counts and robust multiple-array average (RMA) values in GSE151158 and GSE106737, respectively. (C) Representative IF images of liver sections stained with anti-IL22 (red). Lower panels: Magnified insets. White arrowheads indicate IL22⁺ cells. Scale bars: 70 μ m (upper panel) and 35 μ m (lower panel); original magnification, 20 \times . (D) Representative liver tissue heatmaps of IL22⁺ cells (scale: blue = 0 [low] to red = 3 [high] cells/100- μ m diameter). Scale bar: 3000 μ m. (E) Total density quantification (counts per mm²) of hepatic IL22⁺ cells in our cohort (n = 20; females = 9 and males = 11) performed by FIJI software. (F) IL22⁺ cells did not co-express the T-cell marker (CD3). Representative IF images of CD3 (red) and IL22 (green) in liver biopsy (Formalin-Fixed Paraffin-Embedded liver section) from a female patient with NAFLD. Merge: No colocalization between IL22⁺ cells and CD3⁺. Scale bars: 50 μ m; original magnification, 20 \times . White arrowheads indicate CD3⁺ T cells (magenta) or IL-22⁺ cells (green). (G) IF detection of CD66b (red) and IL22 (green) in liver biopsy specimen (Formalin-Fixed Paraffin-Embedded liver section) from a female patient with NAFLD. Yellow rectangles and/or yellow arrowheads in the merge section of panel F indicate IL22-producing neutrophils (CD66b⁺ IL22⁺). Scale bar: 35 μ m; original magnification, 20 \times . Data are expressed as means \pm SD for 9–24 patients per group; Mann-Whitney test. * P < .05 and *** P < .001. Each dot on the bar graphs represent 1 male (triangle) or female (circle) patient. DAPI, 4',6-diamidino-2-phenylindole.

difference in the hepatic frequency of IL17A-producing Th17 (IL17A⁺ IL22⁻ CD4⁺) between HFD-fed female mice compared with controls (mean, 1.1 vs 0.80; P = .5714) (Figure 3D and E), which may suggest a low grade of NASH-

related inflammation. However, the frequency of IL22-producing Th17 (IL22⁺ IL17A⁺ CD4⁺) was significantly different between these 2 groups (P < .05) (Figure 3D and E). Altogether, these data suggest that IL22 expression is

Table 1. NAFLD Patient Demographics and Clinical Characteristics

	Women patients (n = 9)	Men patients (n = 11)
Age, y	50.11 ± 14.39	49.09 ± 11.65
Weight, kg	88.89 ± 20.92	96.86 ± 23.57
ALT level, IU/L	66.67 ± 28.18	75.33 ± 60.64
NAS score criteria		
Hepatic steatosis	1.889 ± 0.928	1.917 ± 0.793
Lobular inflammation	1.444 ± 0.527	1 ± 0.8528
Hepatocyte ballooning	1.444 ± 0.8819	1.083 ± 0.793
Total NAS score	4.889 ± 1.616	4 ± 2.045
Fibrosis score		
NASH CRN criteria	2.778 ± 1.093	1.917 ± 1.165

NOTE. Data are presented as means ± SD. CRN, Clinical Research Network.

up-regulated in livers of HFD-fed female mice compared with males with heterogenous cellular source(s), including T cells.

HFD-Fed IL22ra1^{-/-} Female and/or Male Mice Developed Weight Gain and Other Metabolic Alterations

Several studies have reported a protective role of IL22 against obesity, adiposity, glucose intolerance, and IR in different HFD-induced NAFLD models.^{39–42} Therefore, we first explored whether endogenous IL22-receptor signaling protects against metabolic abnormalities associated with NAFLD in our model. IL22ra1^{-/-} female mice started to show significantly higher weight gain after 9 weeks (mean

difference, 1.843; $P = .025$) on HFD and up to the termination point (30 weeks) (mean difference, 2.160; $P = .004$) compared with WT (Figure 4A). This was associated with worsened glucose intolerance and insulin resistance at 30 weeks (Figure 4C and E). In males, significantly higher weight gain also was observed in IL22ra1^{-/-} male mice compared with WT, starting from 12 weeks (mean difference, 2.567; $P = .019$) and up to 30 weeks (mean difference, 2.956; $P = .006$) (Figure 4B). Although this was associated with increased insulin resistance at 30 weeks, there was no difference in glucose intolerance (Figure 4D and F). Moreover, HFD-fed IL22ra1^{-/-} female mice had markedly higher fat mass, liver index, and hepatic steatosis compared with WT (Figure 5A, E, and G), with no difference in their lean mass (Figure 5C). Similar to females, HFD-fed IL22ra1^{-/-}

Table 2. Individual Demographics and Clinical Characteristics of 20 Patients (9 Women and 11 Men) With NAFLD Analyzed in This Study

Patient	Diagnosis	Sex	Age, y	Weight, kg	ALT level, IU/mL	Fibrosis grade (Clinical Research Network)	H&E (total NAS score)	IF IL22 ⁺ cells
Men (N = 11)								
LB051	NAFLD	M	62	62	53	F2	6	✓
LB054	NASH	M	41	124	249	F3	5	✓
LB059	NASH	M	52	80	66	F0	1	✓
LB078	NASH	M	57	93.2	195	F2	2	✓
LB084	NAFLD	M	33	76	138	F1–F2	5	✓
LB099	NAFLD	M	66	N/A	12	F1	2	✓
LB102	NASH	M	38	101	65	F0	3	✓
LB123	NAFLD	M	52	102	35	F3	5	✓
LB125	NAFLD	M	43	140	196	F3	6	✓
LB130	NAFLD	M	35	81	115	F2	6	✓
LB133	NAFLD	M	61	109.4	16	F1	1	✓
Women (N = 9)								
LB062	NASH	F	59	100.4	58	F4	5	✓
LB076	NASH	F	25	100	138	F1	6	✓
LB079	NAFLD	F	52	55	23	F4	2	✓
LB093	NASH	F	37	N/A	19	F2	6	✓
LB097	NASH	F	62	89	204	F3–F4	3	✓
LB118	NASH	F	40	120	45	F2	5	✓
LB119	NASH	F	73	93	51	F4	6	✓
LB128	NASH	F	51	63	94	F2	7	✓
LB131	NASH	F	52	90.7	46	F3–F4	4	✓

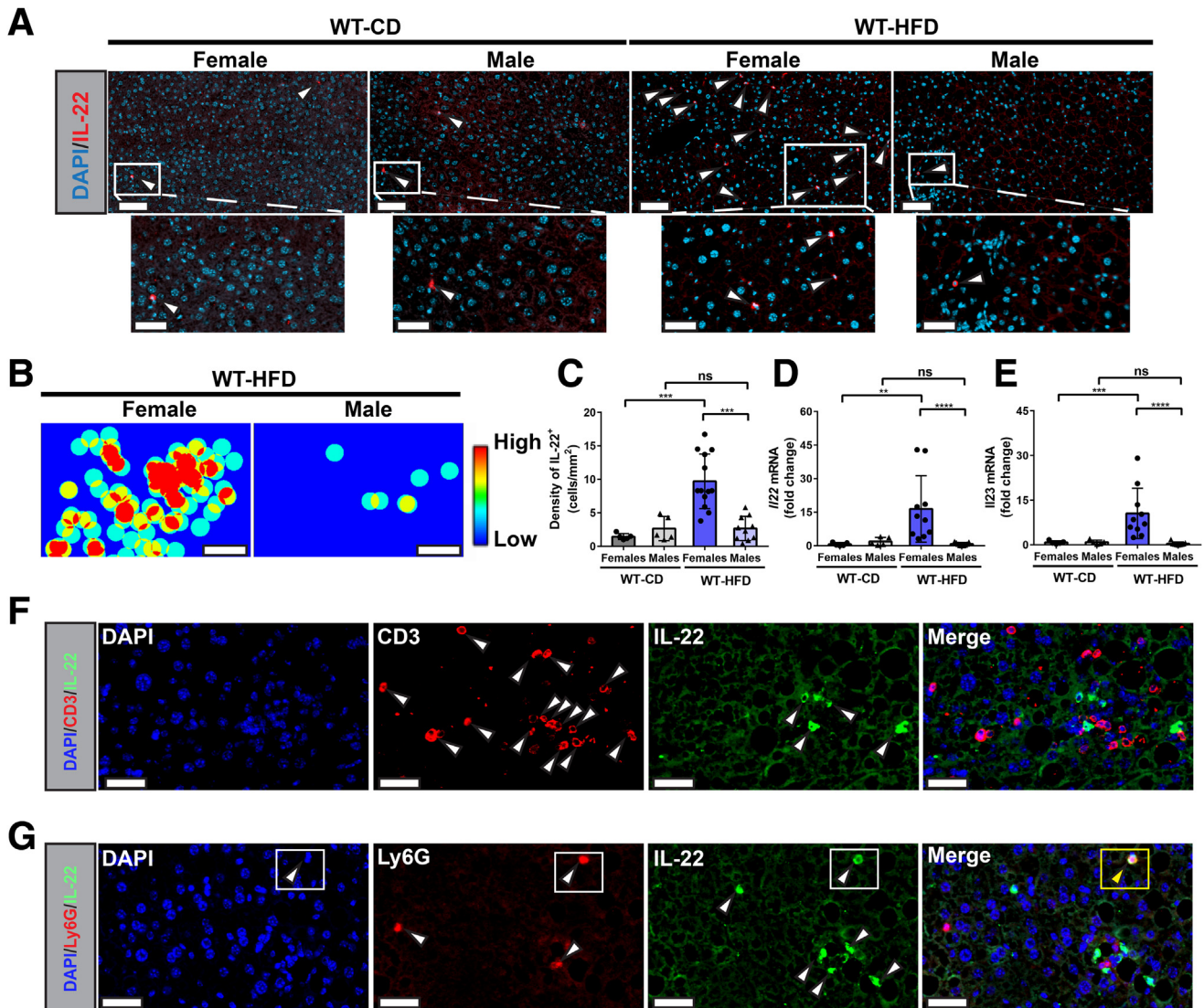


Figure 2. Increased density of IL22⁺ cells in livers of WT HFD-fed female mice compared with males. C57BL/6N male (*triangle*) and female (*circle*) mice were fed a HFD or chow diet (CD) for 30 weeks as described in the Materials and Methods section. (A) Representative IF images of liver sections stained with anti-IL22 (red). *Lower panels*: Magnified *insets*. *White arrowheads* indicate IL22⁺ cells. *Scale bars*: 70 μ m (upper panel) and 35 μ m (lower panel); original magnification, 20 \times . (B) Representative liver tissue heatmaps of IL22⁺ cells (scale: blue = 0 [low] to red = 3 [high] cells/100- μ m diameter). *Scale bar*: 300 μ m. (C) Total density quantification (counts per mm²) of hepatic IL22⁺ cells performed by FIJI software. (D and E) Hepatic *Il22* and *Il23* mRNA expression normalized to ribosomal 28s. Data are expressed as fold change. *White arrowheads* indicate CD3⁺ T cells (Red) or IL-22⁺ cells (green). (F) IL22⁺ cells did not co-express the T-cell marker (CD3). Representative IF images of CD3 (red) and IL22 (green) in Formalin-Fixed Paraffin-Embedded liver sections of HFD-fed WT female mice for 30 weeks. *Merge*: No colocalization between IL22⁺ cells and CD3⁺. *Scale bars*: 35 μ m; original magnification, 20 \times . (G) IF detection of IL22⁺ (green) and Ly6G⁺ (red) cells in liver section (Formalin-Fixed Paraffin-Embedded section) of WT female mouse fed a HFD for 30 weeks. The *rectangle* in the *middle panel* shows the IL22-producing neutrophils (Ly6G⁺ IL22⁺) in the merge. *Scale bar*: 35 μ m; original magnification, 20 \times . *White arrowheads* indicate CD3⁺ T cells (Red) or IL-22⁺ cells (green). Data are expressed as means \pm SD ($n = 5$ –12 mice per group, data were pooled from 3 independent experiments). Mann–Whitney test. ** $P < .01$, *** $P < .001$, and **** $P < .0001$. DAPI, 4',6-diamidino-2-phenylindole.

male mice developed higher adiposity and lean mass compared with WT at 30 weeks, although the difference in fat mass did not reach statistical significance (Figure 5B and D). In addition, no difference was detected between HFD-fed IL22ra1^{-/-} male mice and WT in terms of liver index and

hepatic steatosis (Figure 5F and H). Taken together, these data suggest that a lack of endogenous IL22-receptor signaling likely promotes metabolic abnormalities, especially weight gain and insulin resistance, associated with NAFLD in female and male mice.

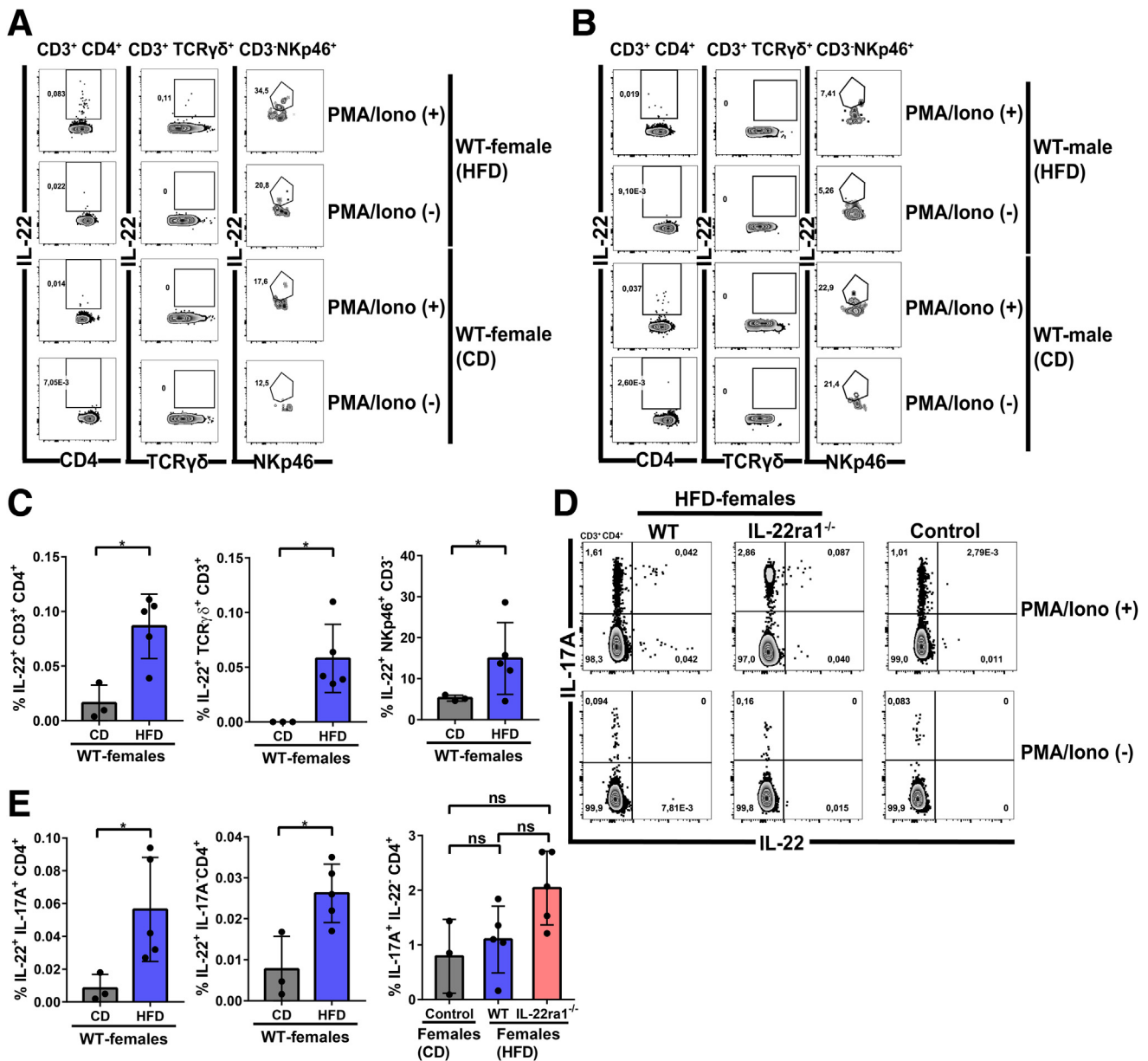


Figure 3. Intrahepatic T cells are major producers of IL22 in HFD-fed WT female mice. Representative flow cytometry plots showing intrahepatic IL22-producing cells: CD4⁺ T cells (IL22⁺CD3⁺CD4⁺), $\gamma\delta$ -T cells (IL22⁺CD3⁺T cell receptor $\gamma\delta$ ⁺), and ILC3s (IL22⁺CD3⁺NKp46⁺) and their frequencies in WT (A) female and (B) male mice. The intrahepatic lymphocytes were extracted from livers of HFD or chow diet (CD)-fed WT female mice at 30 weeks, and then stimulated with/without PMA/ionomycin (PMA/Iono) for 5 hours. (C) The frequency quantification of IL22-producing CD4⁺ T cells, $\gamma\delta$ -T cells, or ILC3s in panel A. (D) Representative flow cytometry plots showing frequencies of IL22 and/or IL17A CD4⁺ T cells, including Th17 (IL22⁺IL17A⁺ CD4⁺ and/or IL17A⁺ IL22⁻ CD4⁺) and Th22 (IL22⁺ IL17A⁻ CD4⁺), in livers of HFD-fed IL22ra1^{-/-} female mice and their WT littermates. (E) The frequency quantification of panel D. Data are expressed as means \pm SD (n = 3–5 mice per group). Mann–Whitney test. *P < .05.

Loss of IL22-Receptor Signaling Exacerbates Liver Injury and NASH-Related Inflammation in HFD-Fed Female Mice

The hepatic inflammatory response is a key driver of human and murine NASH progression because it promotes advancement of hepatic fibrogenesis, which eventually can lead to cirrhosis.⁷ Given that the role of endogenous IL22 in NASH-related inflammation remains unknown, we asked whether the increase in endogenous IL22 expression in the

fatty livers of WT female mice protected against NASH-related liver injury and inflammation. Interestingly, HFD-fed IL22ra1^{-/-} female mice developed more pronounced liver injury compared with WT, as shown by serum alanine aminotransferase (ALT) and histologic assessment of total NAS score (Figure 6A–C). However, there was no significant difference in the individual pathologic categories that make up the NAS score (steatosis, lobular inflammation, and hepatocyte ballooning) between these 2 groups (Figure 6C).

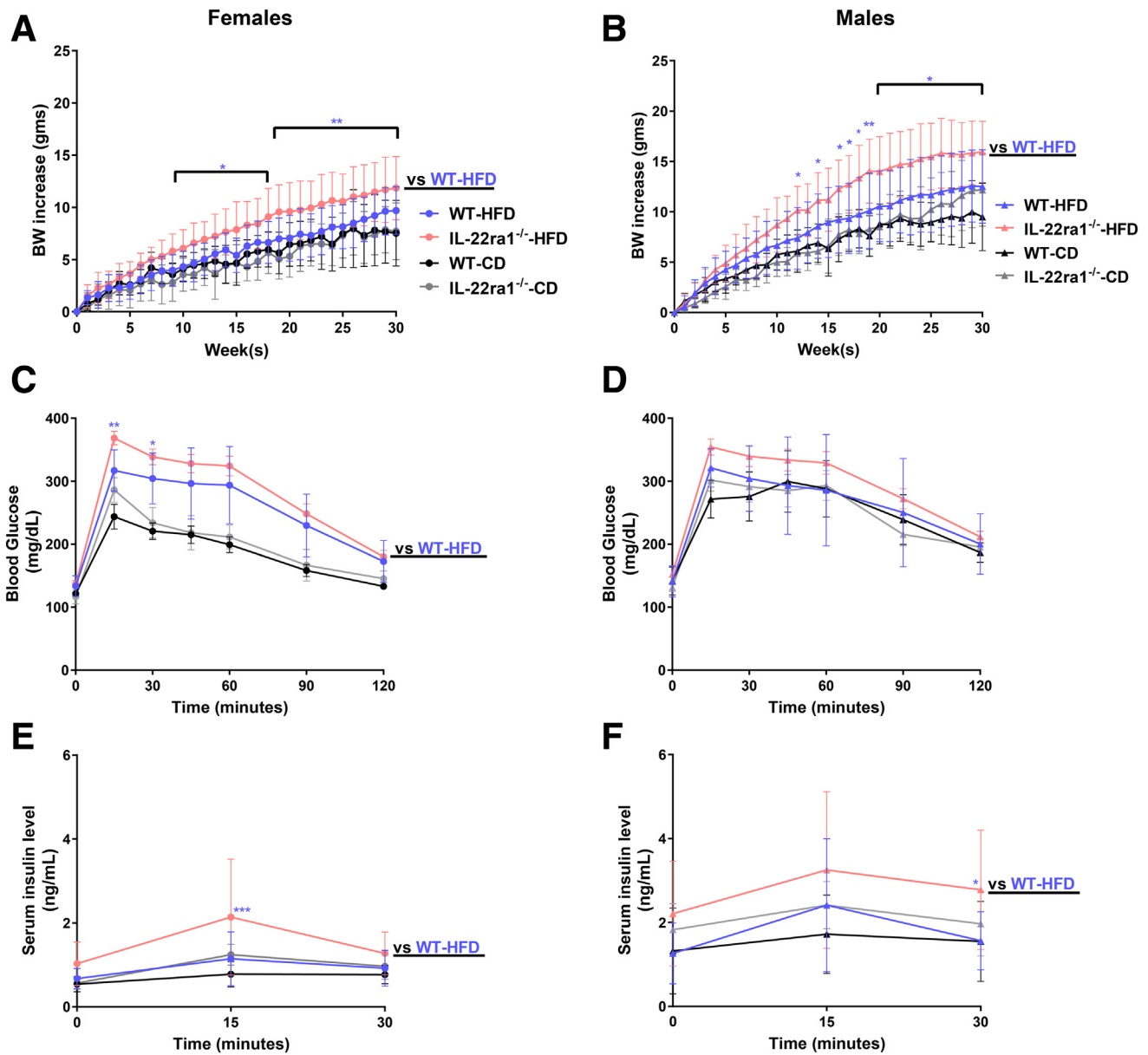


Figure 4. HFD-fed IL22ra1^{-/-} female and/or male mice developed significant weight gain and insulin resistance compared with their WT littermates at 30 weeks. IL22ra1^{-/-} female (circle) or male mice (triangle) and their WT littermates were fed a HFD or chow diet (CD) for 30 weeks. (A and B) Measurements of total body weight gain (in grams) over time. (C and D) Intraperitoneal glucose tolerance test at 30 weeks. (E and F) Measurements of serum insulin at 30 weeks for (A, C, and E) female and (B, D, and F) male mice. Data are expressed as means \pm SD for 8–22 mice per group/sex (data were pooled from 3 independent experiments). (A and B) A 2-way repeated-measures analysis of variance followed by a post hoc test (Holm–Sidak multiple comparisons test) was used. (C and D) Regular 2-way analysis of variance followed by a post hoc test (Holm–Sidak multiple comparisons test) was used. * $P < .05$, ** $P < .01$, and *** $P < .001$. BW, body weight.

One of the characteristic hallmarks of NASH-associated inflammation is the hepatic infiltration of macrophages and neutrophils.^{7,22,47–49} An increase in macrophages/Kupffer cells is associated positively with NASH severity in human beings and mice with NAFLD.^{48,50} Activation of macrophages/Kupffer cells promotes release of several proinflammatory cytokines (eg, IL6) and profibrogenic cytokines (eg, tumor growth factor β (TGF- β)) that exacerbate the inflammatory response in NASH and enhance fibrosis progression by inducing HSC activation.^{7,49,50} Furthermore,

neutrophil infiltration in NASH is associated with increased expression of the myeloperoxidase (MPO) enzyme, which promotes fibrosis progression via activation of HSCs and aggravation of hepatocyte death.^{9,22,47,51} Therefore, using IF, we examined the hepatic infiltration of macrophages (F4/80⁺) and neutrophils (MPO⁺) in our NAFLD model. Hepatic F4/80 and MPO-positive areas were significantly higher in HFD-fed IL22ra1^{-/-} female mice compared with WT (Figure 6A, D, and E). In contrast, we did not observe major differences in liver injury (ALT levels and NAS scores)

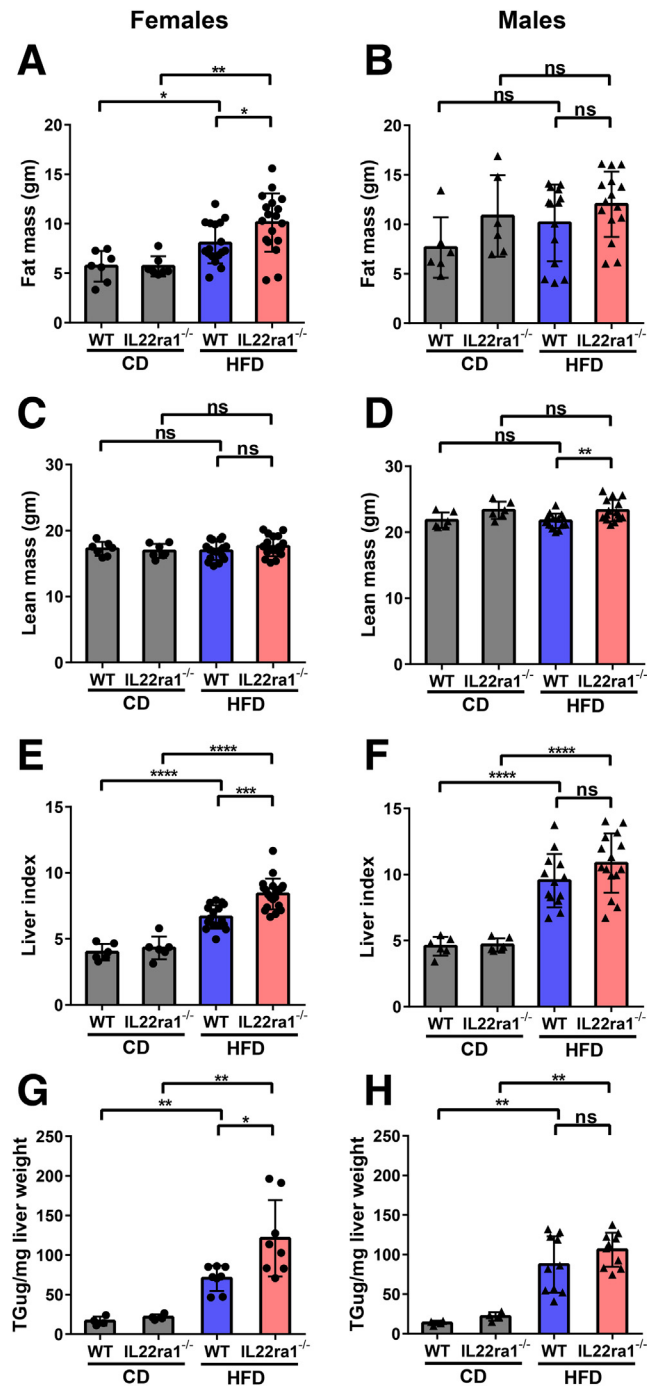


Figure 5. HFD-fed female and/or male mice developed adiposity and hepatic steatosis at 30 weeks. (A and B) Measurements of fat mass (in grams), (C and D) lean mass (in grams), (E and F) liver index (liver/body weight ratio), and (G and H) liver TG level (ug/mg liver weight) at 30 weeks for (A, C, E, and G) female and (B, D, F, and H) male mice. Data are expressed as means \pm SD ($n = 4$ –18 mice per group/sex, data were pooled from 3 independent experiments). Mann–Whitney test. * $P < .05$, ** $P < .01$, *** $P < .001$, and **** $P < .0001$. CD, chow diet.

(Figure 7A–C) and inflammation (F4/80⁺ and MPO⁺ areas) between male HFD-fed IL22ra1^{-/-} mice vs WT (Figure 7A, D, and E). Then, we sought to determine the makeup of other immune cells in the livers and spleen of HFD-fed IL22ra1^{-/-} and WT female or male mice by flow cytometry (Figures 8 and 9). There was a large increase in the numbers of all CD3⁺ T-cell subsets, CD19⁺ B cells, and NK-T cells (CD3⁺ NK1.1⁺), but not NK cells (CD3⁺CD19⁻NK1.1⁺), in the livers and spleens of HFD-fed IL22ra1^{-/-} female mice, but not males, compared with WT (Figure 8B–E). Intriguingly, this was in parallel with an increase in the number of macrophages (CD11b⁺ Ly6C⁻ Ly6G⁻ and F4/80⁺), monocytes (CD11b⁺ Ly6C^{hi} Ly6G⁻), and neutrophils (CD11b⁺ Ly6C^{int+} Ly6G^{hi+}) in the livers and spleens of HFD-fed IL22ra1^{-/-} female mice, but not males, compared with WT (Figure 9B–E). On the other hand, there was no change in the number of dendritic cells (CD11b⁺ Ly6C^{low} Ly6G⁻ F4/80⁻ CD11c⁺) in any of the 4 groups of mice studied (Figure 9B–E). Furthermore, the hepatic mRNA expression of proinflammatory cytokines (*Il6*, tumor necrosis α , *Il1 β*) and inflammatory (C-X-C motif) and (C-C motif) chemokine ligands (*Cxcl-1*, *Cxcl-10*, *Ccl2*, and *Ccl3*) were remarkably higher in HFD-fed IL22ra1^{-/-} female mice than WT (Figure 10A, C, and E). Nonetheless, both HFD-fed IL22ra1^{-/-} male mice and WT had generally comparable profiles of hepatic proinflammatory gene expression except *Ccl2* and *Ccl3* (Figure 10B, D, and F). Collectively, these findings suggest that a lack of endogenous IL22-receptor signaling exacerbates NASH-related liver injury and inflammation in HFD-fed female mice, but not males.

Lack of IL22-Receptor Signaling Promotes Progression of NASH-Related Fibrosis in HFD-Fed Female, but Not Male, Mice

Hepatic fibrosis is initiated by activation of HSCs to transdifferentiate into myofibroblasts characterized by marked up-regulation of type I collagen, α -smooth muscle actin (Actin alpha 2 *Acta2*), and desmin.^{52,53} Thus, based on our findings (Figures 6–10), we sought to determine whether lack of endogenous IL22-receptor signaling in female or male mice will modulate progression of NASH-related fibrosis. As expected, HFD-fed IL22ra1^{-/-} female mice developed advanced NASH-related fibrosis (chicken wire-like perisinusoidal fibrosis) compared with WT, as illustrated by collagen type I deposition, α -smooth muscle actin (α -SMA), and desmin-positive areas measured by picrosirius red (PSR) staining and IF, respectively (Figure 11A, B, D, and E). In addition, the fibrosis grade was evaluated blindly by an expert pathologist and was consistent with PSR-positive area data (Figure 11C). In male mice, there was no difference in liver fibrosis markers and grade between HFD-fed IL22ra1^{-/-} and WT mice (Figure 12A–E). Next, we examined the mRNA expression levels of the profibrogenic genes *Col1a1*, *Tgfb β* , *Acta2*, and *Loxl2* in all groups

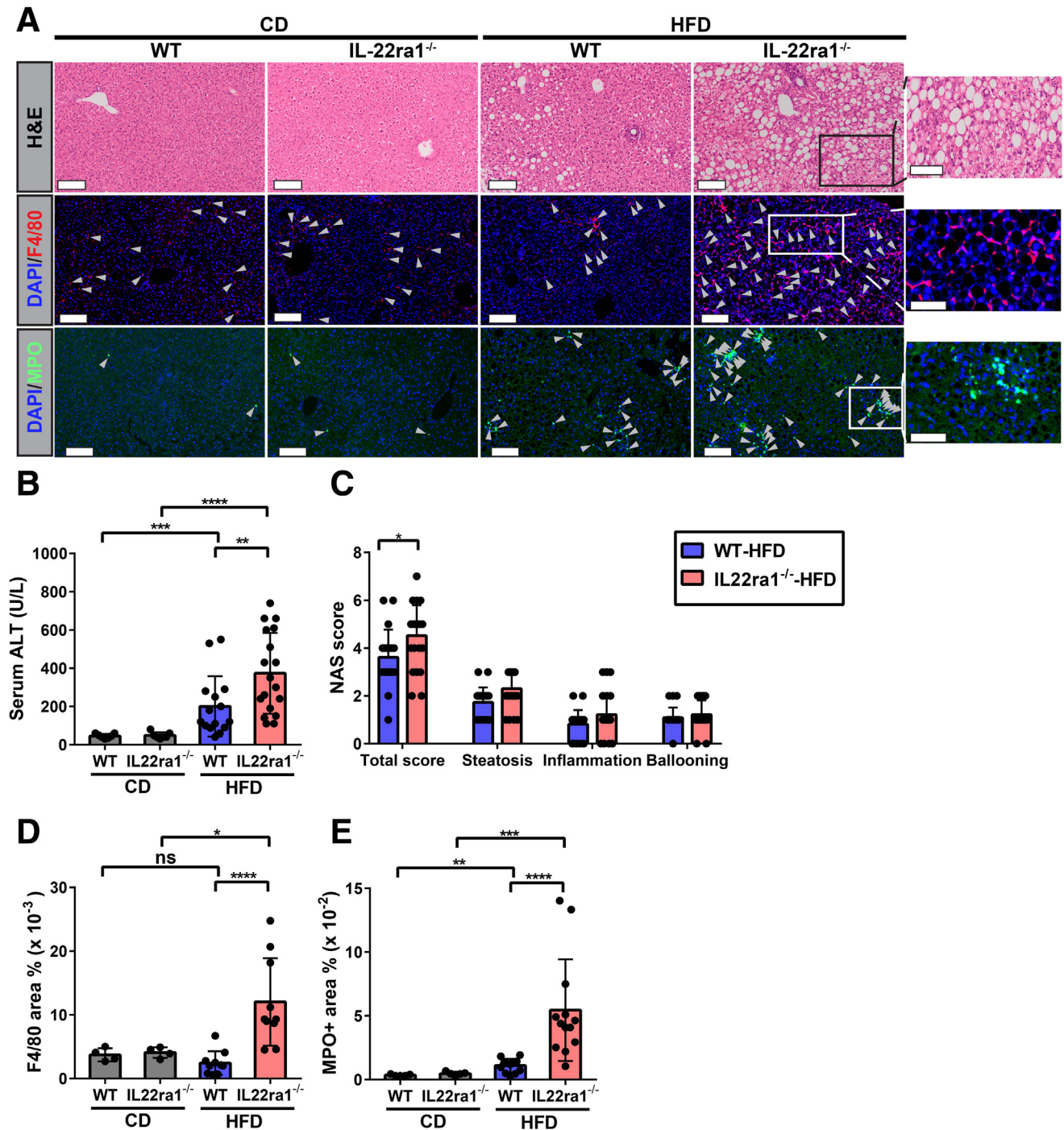


Figure 6. Lack of IL22-receptor signaling exacerbates liver injury and degree of inflammation-induced NASH in HFD-fed female mice. IL22ra1^{-/-} female or male mice and their WT littermates fed on either HFD or chow diet (CD) for 30 weeks. (A) Representative microscopic view of liver sections from IL22ra1^{-/-} and WT female mice stained with H&E and IF staining of macrophage marker F4/80⁺ (red cells are delineated by *arrowheads*) and the neutrophil marker, MPO⁺ (green cells delineated by *arrows*). Scale bars: 100 μ m; original magnification, 20 \times . The *right-most panels* are magnified *insets*. Scale bars of insets 50 μ m for the H&E image and 35 μ m for both MPO⁺ and F4/80⁺ IF images. (B) Measurements of serum ALT level. (C) Blinded pathologic evaluation of NAS score (steatosis grade, lobular inflammation, and hepatocyte ballooning) by an expert pathologist. (D and E) Visiopharm quantification of (D) F4/80⁺ and (E) MPO⁺ areas in livers of female mice. Data are expressed as means \pm SD for 5–22 mice per group (data were pooled from 3 independent experiments). Mann–Whitney test. * $P < .05$, ** $P < .01$, *** $P < .001$, and **** $P < .0001$. DAPI, 4',6-diamidino-2-phenylindole.

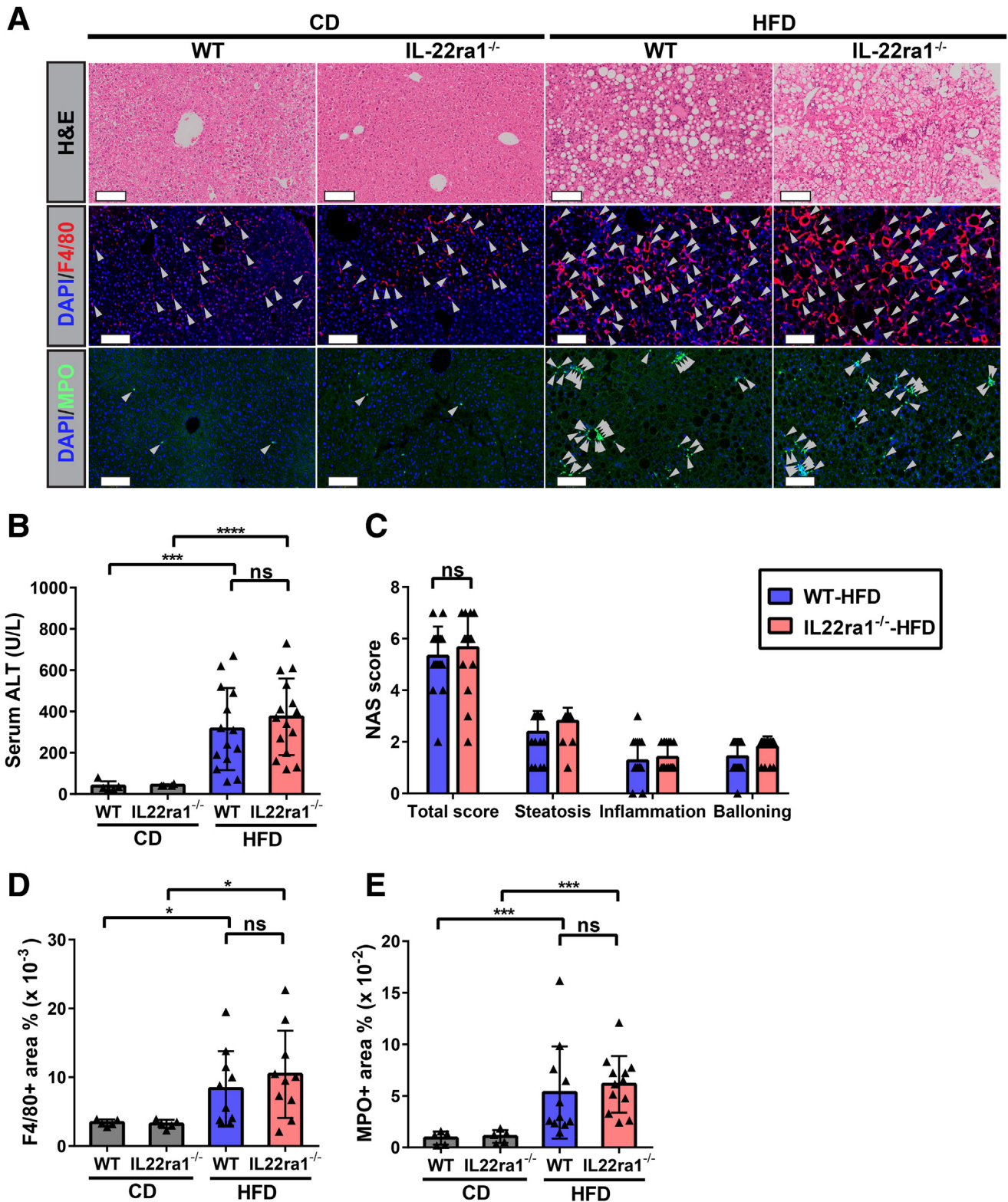


Figure 7. HFD-fed IL22ra1^{-/-} male mice have a comparable profile of inflammation-induced NASH compared with their WT littermates. (A) Representative microscopic view of liver sections of IL22ra1^{-/-} and WT male mice stained with H&E stain and IF staining of macrophage marker F4/80⁺ (red cells delineated by arrowheads) and the neutrophil marker MPO⁺ (green cells delineated by arrowheads). Scale bars: 100 μm; original magnification, 20×. (B) Measurements of serum ALT level. (C) Blinded pathologic evaluation of NAS score (steatosis grade, lobular inflammation, and hepatocyte ballooning) by an expert pathologist. Visiopharm quantification of (D) F4/80⁺ and (E) MPO⁺ areas in livers of male mice. Data are expressed as means ± SD for 5–20 mice per group (data were pooled from 3 independent experiments). Mann–Whitney test. **P* < .05, ****P* < .001, and *****P* < .0001. CD, chow diet; DAPI, 4',6-diamidino-2-phenylindole.

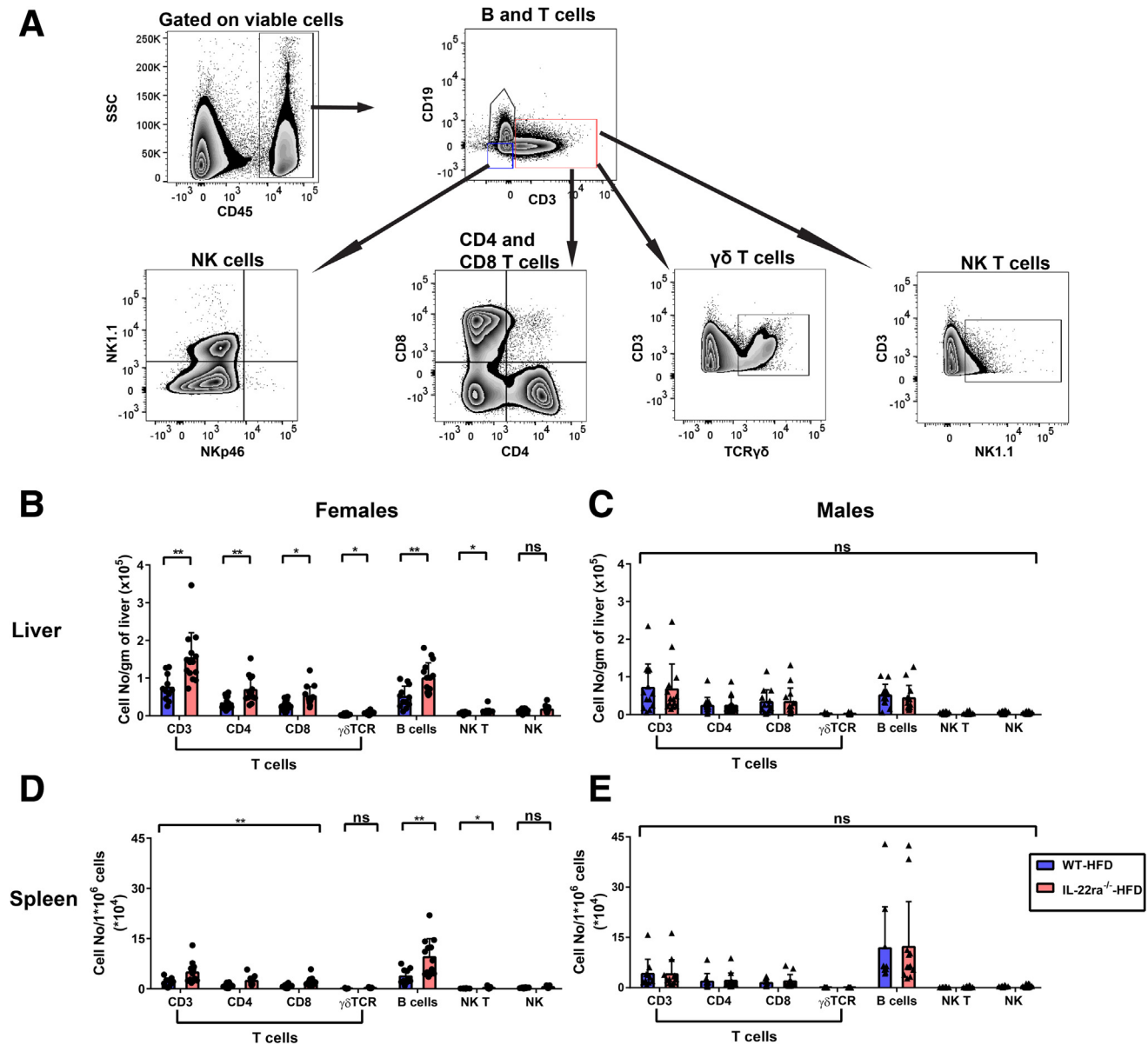


Figure 8. HFD-fed IL22ra1^{-/-} female mice, but not males, develop an increase in the absolute number of adaptive immune cells in their livers and spleen compared with their WT littermates at 30 weeks. IHLs and splenocytes were extracted from fatty livers and spleen of IL22ra1^{-/-} and WT female or male mice, respectively, and analyzed by flow cytometry. (A) Representative FACS plot showing an outline for the gating strategy of B cells (CD45⁺ CD19⁺ CD3⁻), T cells (CD45⁺ CD3⁺ CD19⁻), NK cells (CD45⁺ CD19⁻ CD3⁻ NK1.1⁺ NKp46⁺), CD4⁺ T cells (CD3⁺ CD19⁻ CD4⁺), CD8⁺ T cells (CD3⁺ CD19⁻ CD8⁺), T cell receptor $\gamma\delta$ T cells (CD3⁺ CD19⁻ T cell receptor $\gamma\delta$ ⁺), and NK-T cells (CD3⁺ CD19⁻ NK1.1⁺). The indicated numbers of cell subsets of (B and C) IHLs and (D and E) splenocytes represent cell number/g of liver and splenocyte number/ 10^6 cells for (B and D) female and (C and E) male mice, respectively. Data are expressed as means \pm SD for 10–13 mice per group/sex (data were pooled from 3 independent experiments). Mann–Whitney test. * $P < .05$ and ** $P < .01$. SSC, side scatter characteristics.

studied. Consistent with the histologic data, these genes were highly up-regulated in the livers of HFD-fed IL22ra1^{-/-} female mice, but not males, compared with WT (Figures 11F–J and 12F–J). Overall, the endogenous IL22-receptor signaling likely delays NASH-related fibrosis progression in HFD-fed female mice, while in males, IL22-receptor signaling seems to play an insignificant role during progression of NASH-related fibrosis.

Endogenous IL22-Receptor Signaling Protects Against HFD-Induced Liver Apoptosis in Female, but Not Male, Mice

Cell death, including apoptosis, is one of the fundamental triggers of NASH progression and has been correlated positively with the development of NASH and fibrosis progression.^{7,54,55} In addition, IL22 induces different anti-apoptotic signals in various experimental models of liver

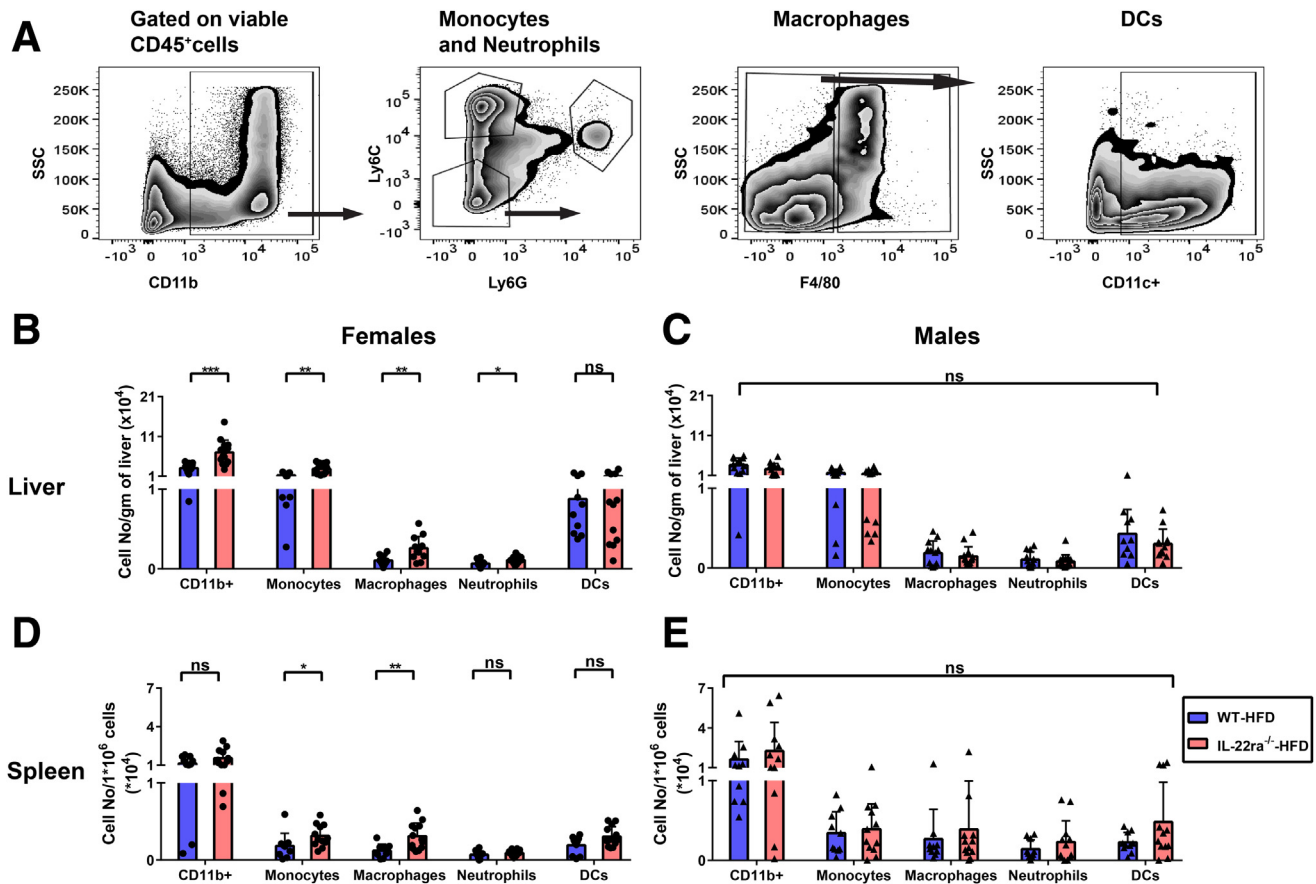


Figure 9. HFD-fed *IL22ra1*^{-/-} female mice, but not males, developed an increase in the absolute number of innate immune cells in their livers and spleen compared with their WT littermates at 30 weeks. IHLs and splenocytes were extracted from fatty livers and spleen of *IL22ra1*^{-/-} and WT female or male mice, respectively, and analyzed by flow cytometry. (A) Representative zebra plots showing an outline for the gating strategy of granulocytes ($CD45^+ CD11b^+$), neutrophils ($CD11b^+ Ly6C^{int} Ly6G^+$), monocytes ($CD11b^+ Ly6C^{hi} Ly6G^-$), macrophages ($CD11b^+ Ly6C^- Ly6G^- F4/80^+$), and dendritic cells (DCs) ($CD11b^+ Ly6C^- Ly6G^- F4/80^- CD11c^+$). The indicated numbers of cell subsets of (B and C) IHLs and (D and E) splenocytes represent the cell number/gram of liver and splenocyte number/ 10^6 cells for (B and D) female and (C and E) male mice, respectively. Data are expressed as means \pm SD for 10–13 mice per group/sex (data were pooled from 3 independent experiments). Mann–Whitney test. * $P < .05$, ** $P < .01$, and *** $P < .001$. SSC, side scatter characteristics.

injury, leading to protection of hepatocytes from apoptosis and enhancement of their survival.^{19,21,22} Thus, to better understand the mechanism(s) underlying the severe liver injury observed in HFD-fed *IL22ra1*^{-/-} female mice, we examined whether hepatocyte cell death is involved. First, we measured the hepatic expression of IL22 downstream target genes *Bcl2*, *Bcl-xL*, *Sod1*, and *Mt2*. *Bcl2* and *Bcl-xL* are anti-apoptotic genes, while *Sod1* (superoxide dismutase 1) and *Mt2* are antioxidant genes.^{19,21,22,42} Interestingly, the mRNA expression levels of these genes were reduced substantially in HFD-fed *IL22ra1*^{-/-} female mice, but not males, compared with WT (Figure 13A and B). Notably, the hepatic expression of these genes was up-regulated in HFD-fed WT female mice compared with those in the chow control group (Figure 13A). Based on these data, we asked whether the IL22 cytokine, detected in livers of females, was biologically active. We therefore measured the hepatic expression of its regulator IL22BP, and it was significantly up-regulated in livers of HFD-fed female mice compared with males,

suggesting tight regulation of IL22 activity by IL22BP (Figure 13C). Nevertheless, the IL22/IL22BP mRNA ratio, which should reflect biologically active IL22, correlated significantly with expression of downstream target genes of IL22 such as *Bcl2*, *Mt2*, and *Sod1* (Figure 13D), suggesting that this regulation process did not limit the overall IL22 activity.

Next, by using the terminal deoxynucleotidyl transferase-mediated deoxyuridine triphosphate nick-end labeling (TUNEL) assay, we explored liver cell death in our NAFLD model. Consistent with serum ALT data, the livers of HFD-fed *IL22ra1*^{-/-} female, but not male, mice showed increased cell death compared with WT (Figure 14A and B). This was reflected by a significant increase in the number of apoptotic bodies observed in HFD-fed *IL22ra1*^{-/-} females compared with WT (Figure 14C). In contrast, we did not detect a difference in the number of apoptotic bodies in the livers of HFD-fed *IL22ra1*^{-/-} male mice compared with WT (Figure 14D). Altogether, these results highlight that the

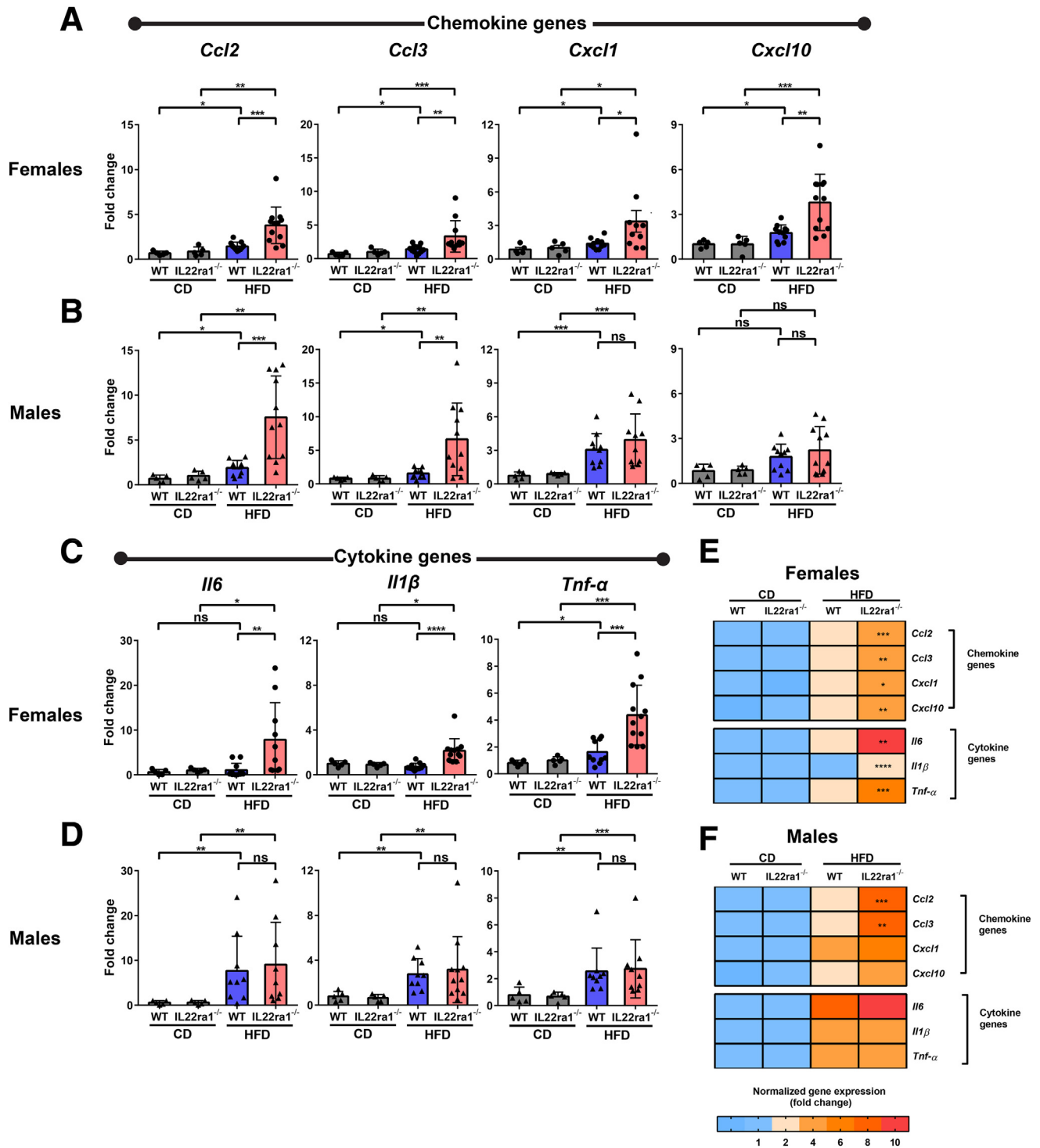
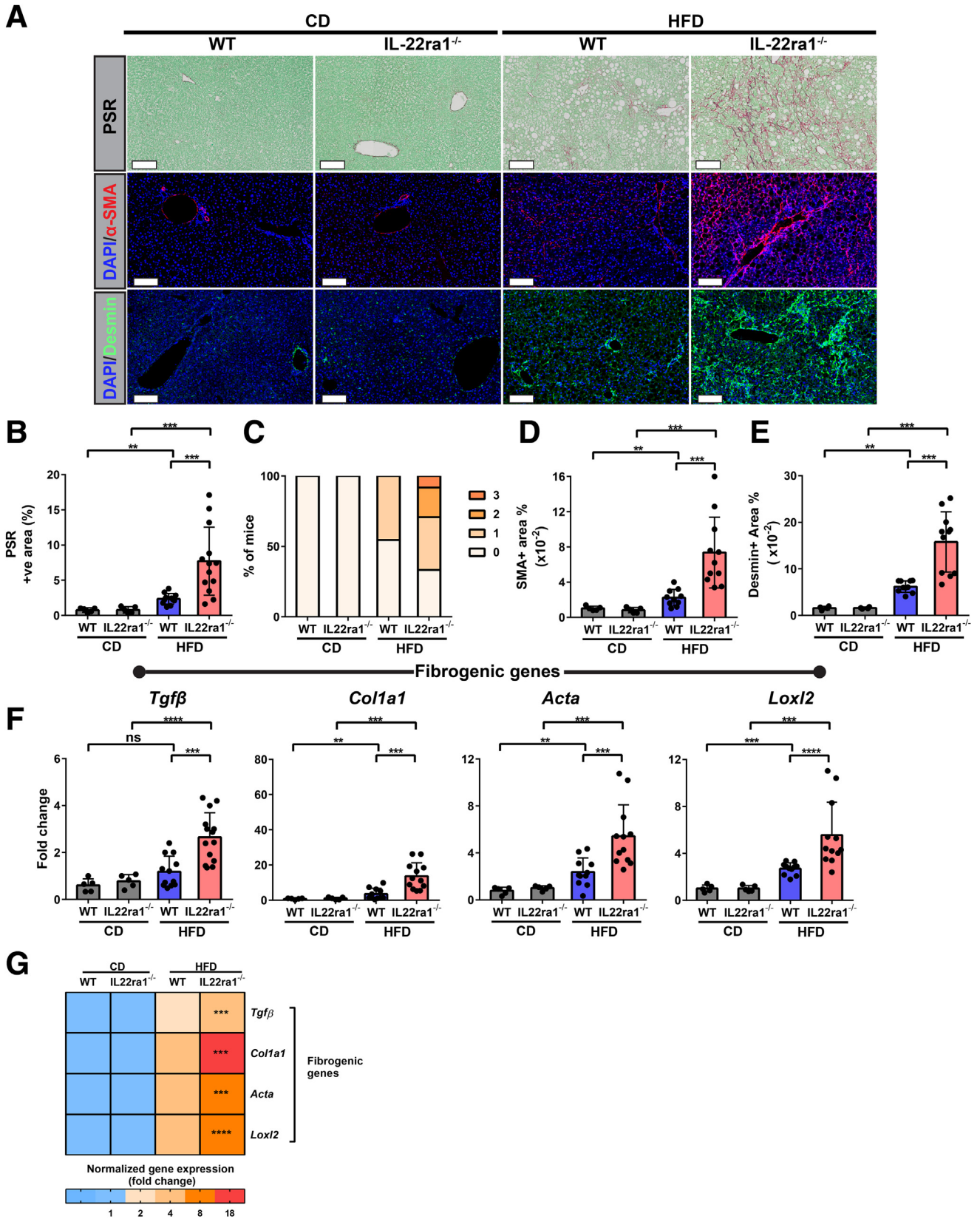


Figure 10. Absence of IL22-receptor signaling results in significant dysregulation of hepatic inflammatory genes in HFD-fed female mice, but not males. Bar graphs of (A and B) proinflammatory chemokine and/or (C and D) cytokine gene expression (normalized to r28s) as indicated and represented as fold change for (A and C) female and (B and D) male mice. (E and F) Heatmaps representing a summary of gene(s) expression in panels A–D for (E) females and (F) males. (E and F) Asterisk(s) indicate statistical significance between the HFD-fed IL22ra1^{-/-} group and their WT littermates. Data are expressed as means ± SD for 5–13 mice per group/sex (data were pooled from 3 independent experiments). Mann–Whitney test. **P* < .05, ***P* < .01, ****P* < .001, and *****P* < .0001. CD, chow diet.



lack of IL22-receptor signaling augments HFD-induced liver cell apoptosis and consequently accelerates the liver injury in female, but not male, mice with NAFLD.

Discussion

In this study, we report sexual dimorphism in hepatic IL22 expression in human beings with NAFLD, in which females expressed higher levels of IL22 gene and protein compared with males. We further validated these findings in HFD-fed mice with NAFLD. The lack of IL22 receptor signaling in female, but not male, mice exacerbated liver injury, apoptosis, inflammation, and, consequently, liver fibrosis. These results suggest a sex-dependent, hepatoprotective role of IL22 in NAFLD.

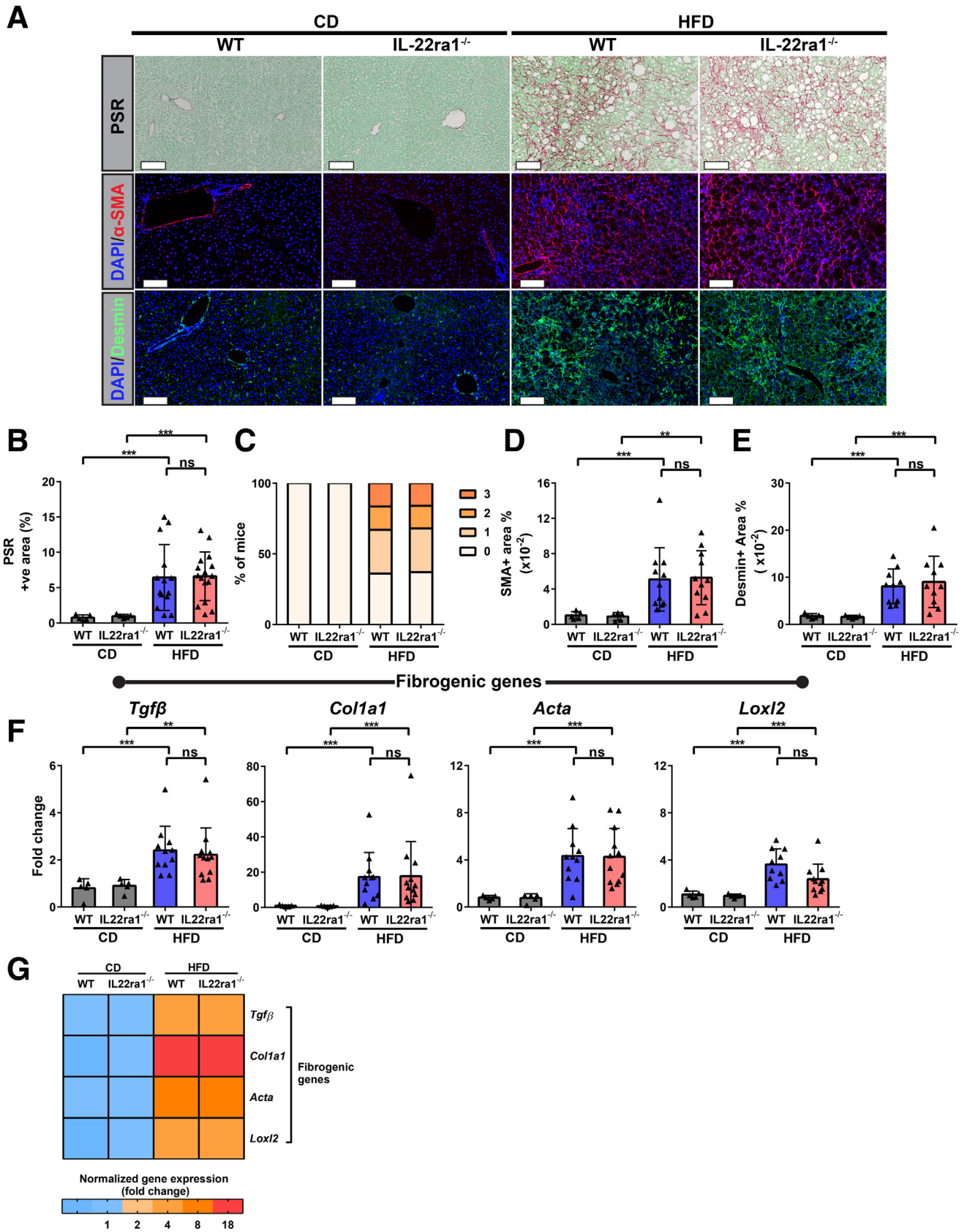
We showed that IL22 was increased significantly in the livers of female subjects and female mice with NAFLD compared with males. In line with this, other *in vivo* studies have reported relatively low serum and hepatic IL22 levels in HFD-fed male mice compared with controls.^{39,41} Interestingly, a recent report showed a comparable plasma IL22 profile between male subjects with NAFLD and healthy controls.⁵⁶ These observations may suggest a regulation of IL22 expression by the female sex hormone estrogen. Indeed, estrogen is known to modulate inflammatory responses in NAFLD, but the underlying mechanisms remain undefined.⁵⁷ For example, significant infiltration of macrophages along with an increase in inflammatory mediators (eg, tumor necrosis factor- α) and liver fibrosis progression were reported in livers of ovariectomized female mice with NAFLD compared with controls.⁵⁸ Furthermore, several observations have suggested cross-regulation between estrogen and IL22. Women with polycystic ovary syndrome, characterized by dysregulated female sex hormones, show significantly lower serum IL22 levels than healthy controls.⁵⁹ In addition, testosterone or dihydrotestosterone reduced IL22 production by female murine splenocytes after stimulation by either lipopolysaccharide or α CD3/CD28.⁶⁰ Moreover, in the imiquimod-induced psoriasis model, administration of estrogen agonists significantly modulated Th-derived IL22, thus aggravating psoriasis symptoms.⁶¹ Further *in vivo* studies are warranted to investigate whether endogenous estrogen regulates hepatic IL22 expression in the context of NAFLD.

We showed that endogenous IL22 was produced by heterogenous cellular populations including Th17, Th22, $\gamma\delta$ -T cells, ILC3s, and neutrophils in the livers of HFD-fed

female mice, where IL22-producing T cells were major producers. In addition, we showed that HFD-fed IL22ra1^{-/-} female mice had relatively higher frequencies of Th17 (IL17A⁺IL22⁻CD4⁺) compared with WT, suggesting an exacerbation of NASH-related inflammation in the absence of IL22-receptor signaling, in parallel with worsening progression of liver fibrosis. In agreement with this, Rolla et al⁴³ reported a hepatoprotective effect of Th22 and amelioration of NASH-related fibrosis, but only in the absence of IL17 (IL17^{-/-} male mice). Thus, our results and those of Rolla et al⁴³ support opposite roles of IL22 (protective) and IL17A (pathogenic) during NASH. However, in comparison with Rolla et al,⁴³ we observed multiple cellular sources of IL22 in the livers of HFD-fed females, not only Th22, which could reflect sex differences and/or utilization of different NASH models (HFD vs a methionine-choline-deficient diet).

We observed beneficial metabolic effects of IL22-receptor signaling against weight gain and IR in HFD-fed WT female or male mice. Wang et al³⁹ observed similar metabolic alterations during diet-induced obesity in IL22R1 knockout, but not in IL22 knockout mice. These data suggest that other IL22RA1 ligands such as IL20 and IL24 may partially mediate these metabolic disorders in IL22ra1-deficient mice upon feeding a HFD.^{11,39} Although ALT levels often correlate with body weight and/or fat mass,⁶² we did not observe a significant difference in ALT levels between HFD-fed IL22ra1^{-/-} and WT male mice. This may be owing to the significant increase in the lean mass in HFD-fed IL22ra1^{-/-} mice compared with WT, while the fat mass was comparable between the 2 groups. In addition, we showed that HFD-fed IL22ra1^{-/-} female mice showed exacerbated hepatic apoptosis and fibrosis progression compared with WT, which seems to be driven by loss of IL22-induced antiapoptotic (*Bcl2*) and antioxidant signals (*Sod1* and *Mt2*). In addition, we observed an up-regulation of the IL22/IL22BP mRNA ratio, reflecting biologically active IL22, in the livers of HFD-fed WT females, which significantly correlated with IL22 target gene expression (*Bcl2*, *Mt2*, and *Sod1*). These data suggest that IL22 still can play a protective role in this NAFLD model, even when it is tightly regulated. In line with this, IL22Fc alleviated oxidative stress-induced hepatocyte death via STAT-3-activating Mt1 and Mt2 in a HFD^{+Cxc1}-induced NASH model, resulting in amelioration of NASH-related fibrosis.²² In addition, our observations support the findings of Zai et al⁴² using liver-targeted delivery of the IL22 gene in a NASH mouse

Figure 11. (See previous page). Loss of IL22-receptor signaling induces severe NASH-related fibrosis in HFD-fed female mice. IL22ra1^{-/-} female mice and their WT littermates were fed either a HFD or chow diet (CD) for 30 weeks. (A) Representative microscopic and IF images of liver sections of IL22ra1^{-/-} female mice and their WT littermates stained with PSR (collagen shown in red), α -smooth muscle actin (α -SMA; shown in red), or desmin (green). Scale bars: 100 μ m; original magnification, 20 \times . (B) FIJI quantification of PSR+ve area in livers of female mice. (C) Blinded pathologic evaluation of liver fibrosis grade of female mice by an expert pathologist. Visiopharm quantification of (D) α -SMA and (E) desmin+ve areas in livers of IL22ra1^{-/-} and WT female mice after HFD or CD treatment for 30 weeks. (F and G) Bar graphs and heatmap of qPCR data of profibrogenic gene expression (normalized to r28s) as indicated and represented as fold change. (G) Asterisk(s) indicate statistical significance between the HFD-fed IL22ra1^{-/-} group and the HFD-fed WT group. Data are expressed as means \pm SD for 5–22 mice per group (data were pooled from 3 independent experiments). Mann–Whitney test. ***P* < .01, and ****P* < .001, *****P* < .0001. DAPI, 4',6-diamidino-2-phenylindole.



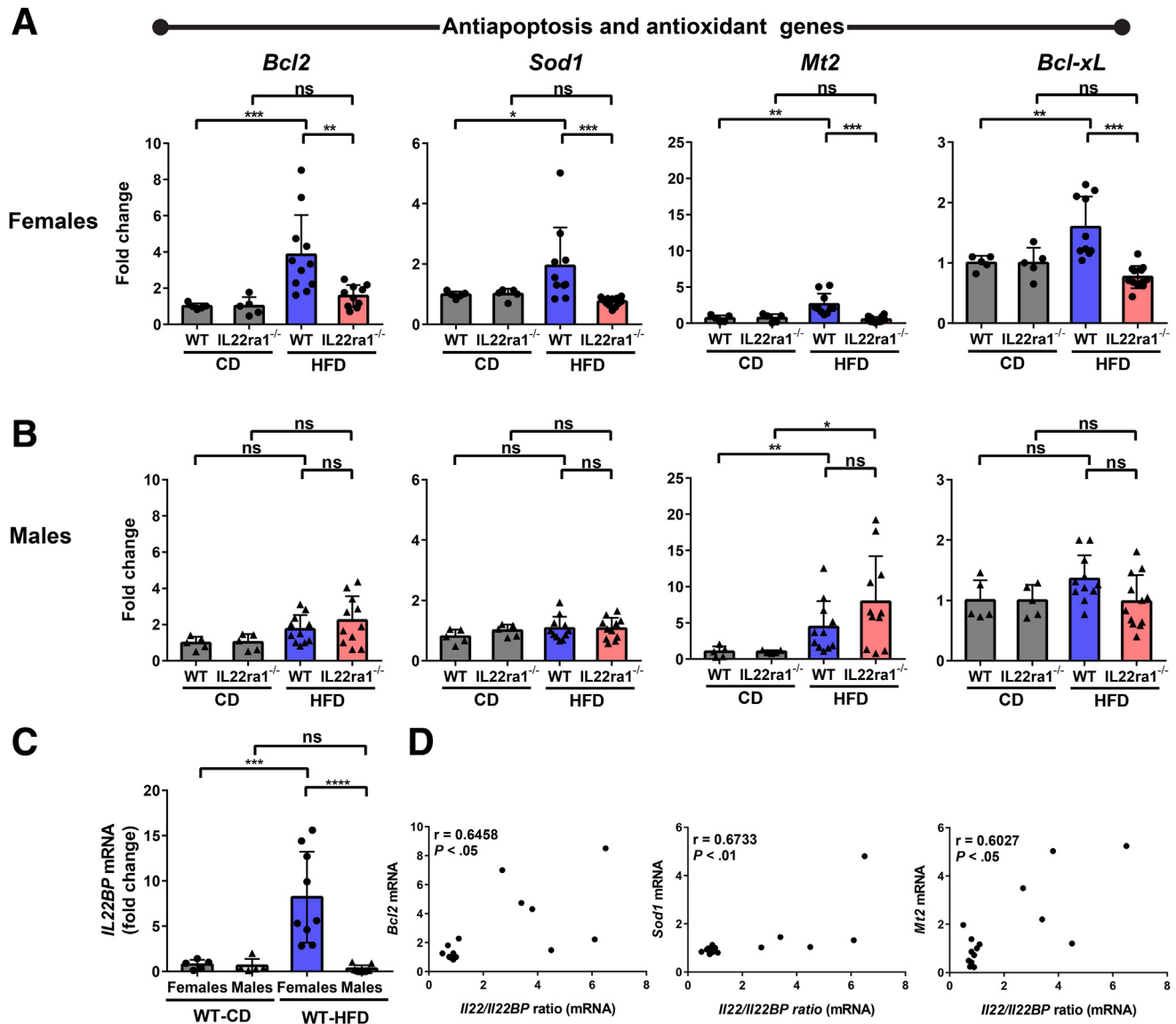


Figure 13. A positive correlation between the hepatic IL22/IL22BP ratio and IL22-induced anti-apoptotic genes in WT female mice. Female (*circle*) and male (*triangle*) mice were fed a HFD or chow diet (CD) for 30 weeks. RNA was extracted from fatty livers of WT female and male mice, converted to cDNA, followed by qPCR. The expression of anti-apoptotic and antioxidant genes as indicated in livers of IL22ra1^{-/-} (A) female or (B) male mice and their WT littermates at 30 weeks. Data were normalized to r28s and represented as fold change. (C) *Il22bp* mRNA expressions were normalized to r28s and represented as fold change. (D) Spearman correlation graphs between the IL22/IL22BP ratio (mRNA) in livers of HFD-fed WT female mice and IL22 downstream target genes: *Bcl2*, *Sod1*, and *Mt2* mRNA. Data are expressed as means \pm SD for 5–12 mice per group/sex (data were pooled from 3 independent experiments). Mann–Whitney test. * $P < .05$, ** $P < .01$, *** $P < .01$, and **** $P < .0001$.

Figure 12. (See previous page). HFD-fed IL22ra1^{-/-} male mice have comparable profiles of NASH-related fibrosis compared with their WT littermates. (A) Representative microscopic and IF images of liver sections of IL22ra1^{-/-} male mice and their WT littermates stained with PSR (collagen in red), α -smooth muscle actin (α -SMA; red), or desmin (green). Scale bars: 100 μ m; original magnification, 20 \times . (B) FIJI quantification of PSR+ve area in livers of male mice. (C) Blinded pathologic evaluation of liver fibrosis grade of male mice by an expert pathologist. Visiopharm quantification of (D) α -SMA and (E) desmin+ve areas in livers of IL22ra1^{-/-} and WT female mice after HFD or chow diet (CD) treatment for 30 weeks. (F and G) Bar graphs and heatmap of qPCR data of profibrogenic gene expression (normalized to r28s) as indicated and represented as fold change. (G) Asterisk(s) indicate statistical significance between HFD-fed IL22ra1^{-/-} group and HFD-fed WT group. Data are expressed as means \pm SD for 5–20 mice per group (data were pooled from 3 independent experiments). Mann–Whitney test. ** $P < .01$, *** $P < .001$, and DAPI, 4',6-diamidino-2-phenylindole.

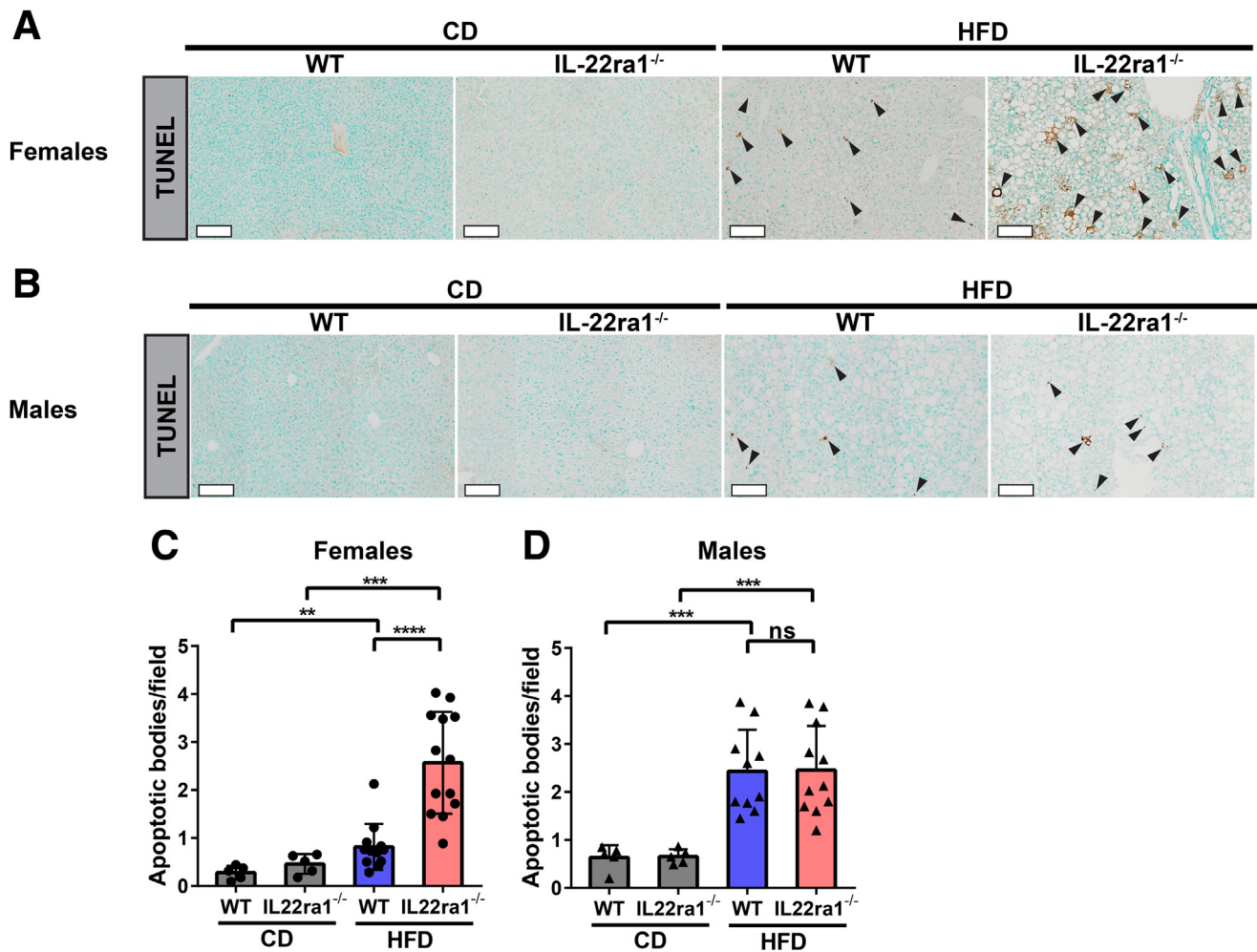


Figure 14. Endogenous IL22-receptor signaling protects against hepatic apoptosis in HFD-fed WT female mice, but not male mice. Representative microscopic view of liver sections stained with TUNEL of IL22ra1^{-/-} and WT (A) female or (B) male mice after HFD treatment for 30 weeks. Scale bars: 100 μ m. Black arrowheads indicate apoptosis. FIJI quantification of apoptotic bodies (count/field) for IL22ra1^{-/-} and WT (C) female or (D) male mice. Data are expressed as means \pm SD for 5–13 mice per group/sex (data were pooled from 3 independent experiments). Mann–Whitney test. ** $P < .01$, *** $P < .001$, and **** $P < .0001$. CD, chow diet.

model, where IL22 activated STAT-3-induced BCL 2 and Nuclear factor erythroid 2-related factor 2-induced superoxide dismutase 1 pathways, resulting in increased hepatocyte survival and proliferation.⁴² Furthermore, our data support the in vitro work from Hamaguchi et al,⁶³ who showed that IL22 inhibited palmitate-induced apoptosis of primary hepatocytes. On the other hand, unlike females, we did not observe significant differences in liver apoptosis or fibrosis between HFD-fed IL22ra1^{-/-} male mice and WT, likely owing to low levels of endogenous IL22 in the livers of HFD-fed male mice. Altogether, our study supports a hepatoprotective function of endogenous IL22-receptor signaling against liver injury in female mice with NAFLD, while the endogenous IL22-receptor signaling appears to play no role against liver injury in male mice with NAFLD.

We and others previously have shown that IL22 has a pathogenic profibrogenic function in human beings and in the CCl₄ and thioacetamide models of chronic toxic liver injury.^{33,34} This effect is mediated through enhancement of

TGF- β signaling in HSCs in a p38 mitogen-activated protein kinase-dependent manner.³³ The different results obtained here, showing a hepatoprotective effect of IL22 in a physiological HFD-induced NAFLD model, may reflect the relatively mild to moderate inflammation and heterogenous fibrosis induced in this NAFLD model, in contrast to a toxin-induced model. This is supported by the low TGF- β mRNA expression in the livers of HFD-fed WT females and could represent a context-dependent function(s) of IL22.

There were a few limitations to this study. First, we used a total body IL22ra1^{-/-} mouse model. Because the IL22RA1 receptor has several ligands such as IL22, IL20, and IL24, our results may have been mildly influenced by a lack of signaling from other IL22RA1 ligands. Future investigation using an IL22^{-/-} model may clarify this issue. Second, the IL22/IL22RA1 axis is crucial for maintaining gut homeostasis, which may have been altered in our model.^{11,64} Microbial translocation and microbial-derived products, resulting from gut dysbiosis, have worsened NASH-related

inflammation in human beings and mice.^{65,66} Therefore, we cannot exclude a potential influence of gut dysbiosis in the promotion of NASH in this model. Further investigation evaluating the microbiome is needed.

In summary, we provide novel evidence of sexual dimorphism in IL22 expression in both human beings and mice with NAFLD. Our data extend previous observations by showing a hepatoprotective function of IL22 in the context of NAFLD, in which IL22-receptor signaling acts in a sex-specific manner and mitigates liver injury, apoptosis, NASH-related inflammation, and fibrosis in female mice. These findings should be considered in clinical trials testing IL22-based therapeutic approaches in treatment of female vs male subjects with NAFLD.²⁸

Methods

Patients

NAFLD patients (n = 20; females = 9 and males = 11) were enrolled through the Hepatology Clinic at the Centre Hospitalier de l'Université de Montréal (CHUM) (Montreal, Canada). This study was approved by the institutional ethics committee (protocol SL09.228) and all participants signed informed consent. The main inclusion criteria of the cohort included a history of alcohol consumption, absence of other chronic liver hepatitis (eg, viral, autoimmune, alcoholic hepatitis), and the NAS score evaluation of liver biopsy specimens. The NAFLD diagnosis was confirmed by an independent pathologist. The demographics and clinical characteristics of the study subjects are summarized in [Table 1](#) and detailed in [Table 2](#). The NAS score and fibrosis grade of participants' liver biopsy specimens were evaluated blindly by an independent pathologist according to the NASH Clinical Research Network criteria.

Microarray Data Sets

Publicly available microarray data sets (GSE151158 and GSE106737) were obtained from 2 published studies, including 2 different cohorts of NAFLD patients.^{44,45} The number of NAFLD patients in GSE151158 and GSE106737 data sets are 9–22 per group and 15–24 per group, respectively. The diagnoses of NAFLD in both studies were based on liver biopsy. Gene expression data along with gene name annotations were downloaded from the Gene Expression Omnibus repository. The normalized values of IL22 mRNA data were expressed as read counts and robust multiple-array average values in GSE151158 and GSE106737, respectively. We stratified the NAFLD patients into females and males in each data set and then assigned the IL22 mRNA normalized value to its corresponding NAFLD patient.

Mice

IL22ra1^{-/-} mice and their WT littermates, of C57BL/6N background, were rederived originally as previously described.³³ Heterozygote couples (IL22ra1^{+/-} × IL22ra1^{+/-}) were used for breeding to generate IL22ra1^{-/-}

mice and WT littermates. Six- to 8-week-old IL22ra1^{-/-} and their WT littermates, including male and female mice, were fed a HFD (40% kcal fat, cat. D17010102I; Research Diets) or chow diet (6.2% kcal fat, Teklad global 18% protein rodent diet; ENVIGO) for 30 weeks. All of the mice were killed at 30 weeks by using pentobarbital (400 mg/kg) and 2% xylocaine. After dissection, the liver, spleen, and blood samples were harvested. All of the animal experimental procedures were approved by the Centre de Recherche du Centre Hospitalier de l'Université de Montréal (CRCHUM) Animal Ethics Committee, Comité Institutionnel de Protection des Animaux (protocol IP18035NSs).

Histology

Human liver biopsy samples were fixed in formalin and processed at the Pathology Laboratory of the CHUM. For mice, liver specimens were fixed in Tissue Fix (cat. no. T-50; Chaptec, Montreal, Quebec, Canada) overnight at 4°C, and finally embedded in paraffin for sectioning (BZ-Histo Services, Inc, Montreal, Quebec, Canada). The 5- μ m-thick Formalin-Fixed Paraffin-Embedded (FFPE) sections were deparaffinized and rehydrated, then stained with PSR stain (cat. no. 365548-5G; Sigma-Aldrich) with Fast green (cat. no. F7252; Sigma-Aldrich) or H&E. The H&E stain was performed by BZ-Histo Services, Inc. TUNEL staining was performed using the TUNEL Assay Kit (horseradish-peroxidase–3,3'-diaminobenzidine tetra hydrochloride kit, ab206386; Abcam) according to the manufacturer's instructions.

IF Staining and Image Analysis

The IF technique and image analysis were performed as previously described.⁶⁷ Briefly, FFPE liver sections (human beings or mice) were deparaffinized and rehydrated. For the antigen retrieval step, the sections were immersed in sodium citrate solution (pH 6) for 10 minutes (with exception to mouse macrophage F4/80 antibody, the incubation was 20 minutes) in an electric high-pressure cooker (Salton). Then, the sections were incubated in 0.1 mol/L glycine for 15 minutes at 25°C to reduce autofluorescence, followed by blocking with 10% human serum, 1% bovine serum albumin, 0.1% Tween 20, and 0.3% Triton-X 100 in phosphate-buffered saline (PBS) solution for 30 minutes. The sections then were incubated with primary antibodies ([Table 3](#)) overnight in 1% bovine serum albumin, 0.1% Tween 20, and 0.3% Triton-X 100 in PBS solution at 4°C. After this, the sections were washed in PBS-Tween and then incubated with the appropriate secondary antibodies ([Table 3](#)) in blocking buffer for 1 hour at 25°C. The sections were mounted in Slow fade Gold mounting media with 4',6-diamidino-2-phenylindole (cat. no. S36938; Thermo Fisher Scientific, Fremont, CA). Finally, the images were acquired at the CRCHUM molecular pathology platform using a whole slide scanner (BX61VS; Olympus). For quantification of IL22-producing cells, FIJI software (version 1.52a, US National Institutes of Health, Bethesda, MD) was used. For all other image analyses, Visiopharm software (Broomfield, CO)

Table 3. List of IF Primary and Secondary Antibodies

Antibodies	Supplier	Catalog number	Concentration
Primary antibodies			
Anti-human IL22	Cloud-Clone Corp	MAC032Hu22	1:100
Anti-human CD66b	Novus Biotechnologies	G10F5	1:100
Anti-mouse IL22	Santa Cruz Biotechnology	SC-14436	1:100
Anti-mouse Ly6G	BioLegend	127602	1:50
Anti-mouse CD3	Abcam	Ab16669	1:100
Anti-human/mouse MPO	R&D	AF3667	1:100
Anti-mouse F4/80	Synaptic System, Germany	397004	1:50
Anti-mouse- α -SMA	Sigma-Aldrich	A2547	1:100
Anti-mouse desmin	Thermo Fisher Scientific, Massachusetts, US	PA5-1670	1:100
Secondary antibodies			
Donkey anti-mouse CF568	Sigma-Aldrich	SAB4600315	1:500
Donkey anti-mouse A647	Thermo Fisher Scientific	A31571	1:500
Donkey anti-mouse IgM A488	Jackson ImmunoResearch	715-545-020	1:300
Donkey anti-goat A568	Thermo Fisher Scientific	A11057	1:500
Chicken anti-rat A678	Thermo Fisher Scientific	A21472	1:250
Donkey anti-rabbit A678	Thermo Fisher Scientific	A31573	1:500
Donkey anti-rabbit A488	Thermo Fisher Scientific	A21206	1:500
Donkey anti- guinea pig A678	Jackson ImmunoResearch	706-605-148	1:500

α -SMA, α -smooth muscle actin.

was used, including tissue detection (tissue vs nontissue), identification, and automatic calculation of the area of interest. Threshold settings based on pixel value was used for generating the calculation of the area of interest.

Body Composition Analysis

Fat/Lean Mass

At 30 weeks, body composition of experimental mice was measured using an EchoMRI-100 Body Composition Analyzer (version 2008.01.18, EchoMRI LLC) at the Rodent Cardiovascular Core Facility of CRCHUM.

Table 4. List of Flow Cytometry Antibodies

Antibody	Supplier	Catalog number
CD45-BV650	BioLegend	103151
CD3-PECF594	BD Bioscience	562286
CD4-BUV496	BD Bioscience	612952
CD8-A700	BioLegend	100730
T cell receptor $\gamma\delta$ -BV421	BD Bioscience	744118
CD19-APC-H7	BD Bioscience	560143
NK1.1-A488	BioLegend	108718
NKp46-SB600	ebioscience	63-3551-82
CD11b-BV421	ebioscience	63-0112-82
Ly6C-PECF594	BD Bioscience	562728
Ly6G-A488	BioLegend	127626
F4/80-BUV395	BD Bioscience	565614
CD11c-Phycoerythrin	BD Bioscience	565592
IL17A-Allophycocyanin	eBioscience	17-7177-81
IL22-Phycoerythrin	eBioscience	12-7227-82

Intraperitoneal Glucose Tolerance Test and Insulin Assay

At 30 weeks, experimental mice were food-deprived for 5 hours with ad libitum access to water. A bolus of glucose (1.5 g/kg) was administered via intraperitoneal injection and glycemia was measured from blood sampled at the tail vein using an Accu-check Performa glucometer (ROCHE) at T0 (before injection), and then at 15, 30, 45, 60, 90, and 120 minutes. Tail vein blood samples were collected via a capillary for insulin assays at 0, 15, and 30 minutes.

Measurement of Liver Triglyceride Levels

Hepatic TG content was evaluated by saponification technique using the Bio-protocole223 (Sigma-Aldrich).⁶⁸ Briefly, liver samples (100–300 mg) were digested in an ethanolic KOH solution overnight at 55°C. After neutralization with MgCl₂, a triacylglycerol glycerol phosphate oxidase kit (cat. no. F6428; Sigma-Aldrich) was used to measure the glycerol content of the samples. Calculations were performed to estimate TG levels, which are presented as a ratio of total liver protein.

Measurement of Serum ALT Levels

Blood samples were drawn using cardiac puncture of the mice and the serum ALT levels were measured at the OPTILAB of the CHUM.

Fibrosis and Apoptosis Quantification

The fibrotic area (PSR-positive area) was determined on the total liver section area and the PSR-positive area was calculated by applying a threshold method in the green channel using Fiji (version 1.52a; US National Institutes of Health) image analysis software. For apoptosis, the number

Table 5. List of Primer Sequences

Gene name	Forward, 5'-3'	Reverse, 5'-3'	Reference
<i>Il22</i>	ATGAGTTTTCCCTTATGGGGAC	GCTGGAAGTTGGACACCTCAA	67
<i>Il6</i>	AGGATACCACTCCCAACAGACCT	CAAGTGCATCATCGTTGTTTCATAC	68
<i>Il1β</i>	GGCAGGCAGTATCACTCATT	GAGGATGGGCTCTTCTTCAAA	69
<i>Tnf-α</i>	ACTCCAGGCGGTGCCTATGT	GTGAGGGTCTGGGCCATAGAA	70
<i>Il23 p19</i>	CCCCCTTCTCCGTTCCAA	GGGCAGCTATGGCCAAAAA	71
<i>Cxcl1</i>	GGATTCACCTCAAGAACATCCAG	ATCTTTTGGACAATTTTCTGAACC	72
<i>Cxcl10</i>	CTTCTGAAAGGTGACCAGCC	GTCGCACCTCCACATAGCTT	73
<i>Ccl2</i>	TCTGGACCCATTCTTCTTGG	TCAGCCAGATGCAGTTAACGC	22
<i>CCl3</i>	GTGGAATCTTCCGGCTGTAG	ACCATGACACTCTGCAACCA	74
<i>Bcl2</i>	ATGCCTTTGTGGAACATATGGC	GGTATGCACCCAGAGTGATGC	76
<i>Bcl-xL</i>	GCTGCATTGTTCCCGTAGAG	GTTGGATGGCCACCTATCTG	77
<i>Sod1</i>	GAGACCTGGGCAATGTGACT	GTTTACTGCGCAATCCCAAT	78
<i>Mt2</i>	GCCTGCAAATGCAAACAATGC	AGCTGCACTTGTCCGGAAGC	22
<i>28s</i>	CGAGATTCCCACTGTCCCTA	GGGGCCTCCCACTTATTCTA	79
<i>Acta2</i>	QT00140119		N/A
<i>Col1a1</i>	QT00162204		
<i>Tgfβ</i>	QT00145250		
<i>Loxl2</i>	QT00129052		

of apoptotic bodies per field were counted in the total liver section area using FIJI software (version 1.52a; US National Institutes of Health), and the average number of apoptotic bodies/field was calculated.

Mouse Intrahepatic Leukocyte Isolation

Intrahepatic leukocytes (IHLs) were isolated from mice livers using a Percoll gradient (cat. no. P1644; Sigma-Aldrich) in isotonic solution. Briefly, mice livers were cut into small pieces and digested in collagenase D (0.025 IU/mL, cat. no. 110088866001; Roche, Laval, Quebec, Canada) and benzonase (10 IU/mL, cat. no. 70664-10KUN; EMD Millipore, Darmstadt, Germany) at 37°C with rotation for 25 minutes. Then, liver tissues were passed through a 70-μm cell strainer (cat. no. 22363548; Thermo Fisher Scientific) followed by centrifugation. The cell pellet then was resuspended in Percoll 40% in 1% Hank's balanced salt solution in sterile water (vol/vol) and layered over Percoll 80% in 1% Hank's balanced salt solution in sterile water (vol/vol), followed by centrifugation without brakes for 25 minutes. Next, IHLs were washed, and red blood cells were lysed using Ammonium-Chloride-Potassium lysing buffer (cat. no. A10492-01; Thermo Fisher Scientific). IHLs were directly stained for surface markers or stimulated with PMA/ionomycin (50 ng/mL, cat. no. P1585 and 1 μg/mL, cat. no. I-0634; Sigma-Aldrich, respectively) in the presence of brefeldin A (5 μg/mL, cat. no. B6542; Sigma-Aldrich) and monensin (5 μg/mL, cat. no. M5273; Sigma-Aldrich) for 5 hours before intracellular cytokine staining.

Mouse Splenocyte Isolation

Mouse spleens were digested by direct passing through a 40-μm cell strainer (cat. no. 22363547; Fisher). Then, the cell suspension was centrifuged and resuspended in

Ammonium-Chloride-Potassium lysing buffer to lyse red blood cells. Splenocytes then were resuspended in RPMI media and filtered. The cells were counted using a hemocytometer and then directly stained for flow cytometry analysis.

Flow Cytometry

IHL and splenocytes were stained as previously described.³³ Briefly, freshly isolated IHLs and splenocytes were washed with flow cytometry buffer (1% heat-inactivated fetal bovine serum and 0.01% azide in PBS), followed by incubation with primary antibodies (Table 4) at 4°C for 30 minutes. Next, the cells were washed with FACS buffer and fixed with 1% paraformaldehyde in PBS and filtered using polystyrene tubes with a cell strainer (Corning Science, Mexico). For intracellular cytokine staining, surface staining was performed first and then the cells were fixed and permeabilized using forkhead box P3 fixation buffer (cat. no. 005523-00; eBioscience). Then, cells were washed twice with washing buffer (eBioscience) and incubated with antibodies for intracellular antigens at 4°C for 30 minutes. For detection of live cells, the Aqua Live/Dead Fixable Dead Cell Stain kit was used (cat. no. L34966; Life Technologies, Burlington, Ontario, Canada). Data were acquired using a multicolor BD LSRII flow cytometer (BD Bioscience) equipped with FACS DIVA software version 8 and analyzed using FlowJo software, version 10 (BD Bioscience).

Real-Time qPCR

Total RNA was isolated and purified from mouse livers using the RNeasy Mini kit plus (cat. no. 74134; QIAGEN, Germany) according to the manufacturer's instructions. Then, 1 μg RNA was reverse-transcribed to complementary DNAs (cDNAs) using the Transcriptor Universal cDNA

Master (cat. no. 05893151001; Roche, Germany) kit. cDNAs were diluted 1:10 with ultrapure water and the relative expression of the mRNA level was measured using real-time qPCR with the Light Cycler 480 SYBR Green I system (cat. no. 04707494001; Roche). r28S was used as the standard housekeeping gene and the $2^{-\Delta\Delta Ct}$ method was applied to calculate the mRNA level. The list of primer sequences used for real-time qPCR are listed in Table 5. Primers for *Tgfb*, *Col1a1*, *Acta2*, and *Lox12* genes were purchased from QIAGEN.

Statistical Analysis

GraphPad Prism 7 (La Jolla, CA) and Sigma plot 14 (version 1.0.23) were used. The Mann–Whitney test was applied to determine differences between 2 groups. Two-way analysis of variance followed by the Holm–Sidak post hoc test was used to determine the differences between groups for glucose intolerance and IR data of mice. Correlations were tested using the Spearman rank correlation and 2-way repeated-measures analysis of variance, followed by the Holm–Sidak post hoc test was used for determining the longitudinal difference in weight gain of mice.

References

1. Younossi Z, Anstee QM, Marietti M, Hardy T, Henry L, Eslam M, George J, Bugianesi E. Global burden of NAFLD and NASH: trends, predictions, risk factors and prevention. *Nat Rev Gastroenterol Hepatol* 2018; 15:11–20.
2. Estes C, Razavi H, Loomba R, Younossi Z, Sanyal AJ. Modeling the epidemic of nonalcoholic fatty liver disease demonstrates an exponential increase in burden of disease. *Hepatology* 2018;67:123–133.
3. Ge X, Zheng L, Wang M, Du Y, Jiang J. Prevalence trends in non-alcoholic fatty liver disease at the global, regional and national levels, 1990–2017: a population-based observational study. *BMJ Open* 2020;10:e036663.
4. Lonardo A, Nascimbeni F, Ballestri S, Fairweather D, Win S, Than TA, Abdelmalek MF, Suzuki A. Sex differences in nonalcoholic fatty liver disease: state of the art and identification of research gaps. *Hepatology* 2019; 70:1457–1469.
5. Zhu L, Martinez MN, Emfinger CH, Palmisano BT, Stafford JM. Estrogen signaling prevents diet-induced hepatic insulin resistance in male mice with obesity. *Am J Physiol Endocrinol Metab* 2014;306:E1188–E1197.
6. Turola E, Petta S, Vanni E, Milosa F, Valenti L, Critelli R, Miele L, Maccio L, Calvaruso V, Fracanzani AL, Bianchini M, Raos N, Bugianesi E, Mercorella S, Di Giovanni M, Craxi A, Fargion S, Grieco A, Cammà C, Cotelli F, Villa E. Ovarian senescence increases liver fibrosis in humans and zebrafish with steatosis. *Dis Model Mech* 2015;8:1037–1046.
7. Hardy T, Oakley F, Anstee QM, Day CP. Nonalcoholic fatty liver disease: pathogenesis and disease spectrum. *Annu Rev Pathol* 2016;11:451–496.
8. Chalasani N, Younossi Z, Lavine JE, Charlton M, Cusi K, Rinella M, Harrison SA, Brunt EM, Sanyal AJ. The diagnosis and management of nonalcoholic fatty liver disease: practice guidance from the American Association for the Study of Liver Diseases. *Hepatology* 2018;67:328–357.
9. Pulli B, Ali M, Iwamoto Y, Zeller MW, Schob S, Linnoila JJ, Chen JW. Myeloperoxidase-hepatocyte-stellate cell cross talk promotes hepatocyte injury and fibrosis in experimental nonalcoholic steatohepatitis. *Antioxid Redox Signal* 2015;23:1255–1269.
10. Taylor RS, Taylor RJ, Bayliss S, Hagström H, Nasr P, Schattner JM, Ishigami M, Toyoda H, Wai-Sun Wong V, Peleg N, Shlomai A, Sebastiani G, Seko Y, Bhala N, Younossi ZM, Anstee QM, McPherson S, Newsome PN. Association between fibrosis stage and outcomes of patients with nonalcoholic fatty liver disease: a systematic review and meta-analysis. *Gastroenterology* 2020;158:1611–1625.e12.
11. Dudakov JA, Hanash AM, van den Brink MR. Interleukin-22: immunobiology and pathology. *Annu Rev Immunol* 2015;33:747–785.
12. Chung Y, Yang X, Chang SH, Ma L, Tian Q, Dong C. Expression and regulation of IL-22 in the IL-17-producing CD4+ T lymphocytes. *Cell Res* 2006; 16:902–907.
13. Mielke LA, Jones SA, Raverdeau M, Higgs R, Stefanska A, Groom JR, Misiak A, Dungan LS, Sutton CE, Streubel G, Bracken AP, Mills KH. Retinoic acid expression associates with enhanced IL-22 production by $\gamma\delta$ T cells and innate lymphoid cells and attenuation of intestinal inflammation. *J Exp Med* 2013; 210:1117–1124.
14. Zindl CL, Lai JF, Lee YK, Maynard CL, Harbour SN, Ouyang W, Chaplin DD, Weaver CT. IL-22-producing neutrophils contribute to antimicrobial defense and restitution of colonic epithelial integrity during colitis. *Proc Natl Acad Sci U S A* 2013;110:12768–12773.
15. Dumoutier L, Lejeune D, Colau D, Renauld JC. Cloning and characterization of IL-22 binding protein, a natural antagonist of IL-10-related T cell-derived inducible factor/IL-22. *J Immunol* 2001;166:7090–7095.
16. Wolk K, Kunz S, Witte E, Friedrich M, Asadullah K, Sabat R. IL-22 increases the innate immunity of tissues. *Immunity* 2004;21:241–254.
17. Andoh A, Zhang Z, Inatomi O, Fujino S, Deguchi Y, Araki Y, Tsujikawa T, Kitoh K, Kim-Mitsuyama S, Takayanagi A, Shimizu N, Fujiyama Y. Interleukin-22, a member of the IL-10 subfamily, induces inflammatory responses in colonic subepithelial myofibroblasts. *Gastroenterology* 2005;129:969–984.
18. Ki SH, Park O, Zheng M, Morales-Ibanez O, Kolls JK, Bataller R, Gao B. Interleukin-22 treatment ameliorates alcoholic liver injury in a murine model of chronic-binge ethanol feeding: role of signal transducer and activator of transcription 3. *Hepatology* 2010;52:1291–1300.
19. Zenewicz LA, Yancopoulos GD, Valenzuela DM, Murphy AJ, Karow M, Flavell RA. Interleukin-22 but not interleukin-17 provides protection to hepatocytes during acute liver inflammation. *Immunity* 2007;27:647–659.
20. Scheiermann P, Bachmann M, Goren I, Zwissler B, Pfeilschifter J, Mühl H. Application of interleukin-22

- mediates protection in experimental acetaminophen-induced acute liver injury. *Am J Pathol* 2013; 182:1107–1113.
21. Radaeva S, Sun R, Pan HN, Hong F, Gao B. Interleukin 22 (IL-22) plays a protective role in T cell-mediated murine hepatitis: IL-22 is a survival factor for hepatocytes via STAT3 activation. *Hepatology* 2004;39:1332–1342.
 22. Hwang S, He Y, Xiang X, Seo W, Kim SJ, Ma J, Ren T, Park SH, Zhou Z, Feng D, Kunos G, Gao B. Interleukin-22 ameliorates neutrophil-driven nonalcoholic steatohepatitis through multiple targets. *Hepatology* 2020; 72:412–429.
 23. Zheng M, Horne W, McAleer JP, Pociask D, Eddens T, Good M, Gao B, Kolls JK. Therapeutic role of interleukin 22 in experimental intra-abdominal *Klebsiella pneumoniae* infection in mice. *Infect Immun* 2016;84:782–789.
 24. Kong X, Feng D, Wang H, Hong F, Bertola A, Wang FS, Gao B. Interleukin-22 induces hepatic stellate cell senescence and restricts liver fibrosis in mice. *Hepatology* 2012;56:1150–1159.
 25. Meng F, Wang K, Aoyama T, Grivennikov SI, Paik Y, Scholten D, Cong M, Iwaisako K, Liu X, Zhang M, Österreicher CH, Stickel F, Ley K, Brenner DA, Kisseleva T. Interleukin-17 signaling in inflammatory, Kupffer cells, and hepatic stellate cells exacerbates liver fibrosis in mice. *Gastroenterology* 2012;143:765–776.e3.
 26. Kudira R, Malinka T, Kohler A, Dosch M, de Agüero MG, Melin N, Haegele S, Starlinger P, Maharjan N, Saxena S, Keogh A, Stroka D, Candinas D, Beldi G. P2X1-regulated IL-22 secretion by innate lymphoid cells is required for efficient liver regeneration. *Hepatology* 2016; 63:2004–2017.
 27. Shen Y, Jin X, Chen W, Gao C, Bian Q, Fan J, Luan J, Cao Z, Guo Z, Gu Y, Liu H, Ju D, Mei X. Interleukin-22 ameliorated acetaminophen-induced kidney injury by inhibiting mitochondrial dysfunction and inflammatory responses. *Appl Microbiol Biotechnol* 2020; 104:5889–5898.
 28. Tang KY, Lickliter J, Huang ZH, Xian ZS, Chen HY, Huang C, Xiao C, Wang YP, Tan Y, Xu LF, Huang YL, Yan XQ. Safety, pharmacokinetics, and biomarkers of F-652, a recombinant human interleukin-22 dimer, in healthy subjects. *Cell Mol Immunol* 2019;16:473–482.
 29. Rothenberg ME, Wang Y, Lekkerkerker A, Danilenko DM, Maciuga R, Erickson R, Herman A, Stefanich E, Lu TT. Randomized phase I healthy volunteer study of UTTR1147A (IL-22Fc): a potential therapy for epithelial injury. *Clin Pharmacol Ther* 2019;105:177–189.
 30. Arab JP, Sehrawat TS, Simonetto DA, Verma VK, Feng D, Tang T, Dreyer K, Yang X, Daley WL, Sanyal A, Chalasani N, Radaeva S, Yang L, Vargas H, Ibacache M, Gao B, Gores GJ, Malhi H, Kamath PS, Shah VH. An open-label, dose-escalation study to assess the safety and efficacy of IL-22 agonist F-652 in patients with alcohol-associated hepatitis. *Hepatology* 2020; 72:441–453.
 31. Zhang Y, Cobleigh MA, Lian JQ, Huang CX, Booth CJ, Bai XF, Robek MD. A proinflammatory role for interleukin-22 in the immune response to hepatitis B virus. *Gastroenterology* 2011;141:1897–1906.
 32. Zhao J, Zhang Z, Luan Y, Zou Z, Sun Y, Li Y, Jin L, Zhou C, Fu J, Gao B, Fu Y, Wang FS. Pathological functions of interleukin-22 in chronic liver inflammation and fibrosis with hepatitis B virus infection by promoting T helper 17 cell recruitment. *Hepatology* 2014; 59:1331–1342.
 33. Fabre T, Molina MF, Soucy G, Goulet JP, Willems B, Villeneuve JP, Bilodeau M, Shoukry NH. Type 3 cytokines IL-17A and IL-22 drive TGF-beta-dependent liver fibrosis. *Sci Immunol* 2018;3.
 34. Wu LY, Liu S, Liu Y, Guo C, Li H, Li W, Jin X, Zhang K, Zhao P, Wei L, Zhao J. Up-regulation of interleukin-22 mediates liver fibrosis via activating hepatic stellate cells in patients with hepatitis C. *Clin Immunol* 2015; 158:77–87.
 35. Xue J, Zhao Q, Sharma V, Nguyen LP, Lee YN, Pham KL, Edderkaoui M, Pandol SJ, Park W, Habtezion A. Aryl hydrocarbon receptor ligands in cigarette smoke induce production of interleukin-22 to promote pancreatic fibrosis in models of chronic pancreatitis. *Gastroenterology* 2016;151:1206–1217.
 36. Lücke J, Sabihi M, Zhang T, Bauditz LF, Shiri AM, Giannou AD, Huber S. The good and the bad about separation anxiety: roles of IL-22 and IL-22BP in liver pathologies. *Semin Immunopathol* 2021;43:591–607.
 37. Kleinschmidt D, Giannou AD, McGee HM, Kempinski J, Steglich B, Huber FJ, Ernst TM, Shiri AM, Wegscheid C, Tasika E, Hübener P, Huber P, Bedke T, Steffens N, Agalioti T, Fuchs T, Noll J, Lotter H, Tiegs G, Lohse AW, Axelrod JH, Galun E, Flavell RA, Gagliani N, Huber S. A protective function of IL-22BP in ischemia reperfusion and acetaminophen-induced liver injury. *J Immunol* 2017;199:4078–4090.
 38. Sertorio M, Hou X, Carmo RF, Dessein H, Cabantous S, Abdelwahed M, Romano A, Albuquerque F, Vasconcelos L, Carmo T, Li J, Varoquaux A, Arnaud V, Oliveira P, Hamdoun A, He H, Adbelmaboud S, Mergani A, Zhou J, Monis A, Pereira LB, Halfon P, Bourlière M, Parana R, Dos Reis M, Gonnelli D, Moura P, Elwali NE, Argiro L, Li Y, Dessein A. IL-22 and IL-22 binding protein (IL-22BP) regulate fibrosis and cirrhosis in hepatitis C virus and schistosome infections. *Hepatology* 2015;61:1321–1331.
 39. Wang X, Ota N, Manzanillo P, Kates L, Zavala-Solorio J, Eidenschenk C, Zhang J, Lesch J, Lee WP, Ross J, Diehl L, van Bruggen N, Kolumam G, Ouyang W. Interleukin-22 alleviates metabolic disorders and restores mucosal immunity in diabetes. *Nature* 2014;514:237–241.
 40. Yang L, Zhang Y, Wang L, Fan F, Zhu L, Li Z, Ruan X, Huang H, Wang Z, Huang Z, Huang Y, Yan X, Chen Y. Amelioration of high fat diet induced liver lipogenesis and hepatic steatosis by interleukin-22. *J Hepatol* 2010; 53:339–347.
 41. Park O, Ki SH, Xu M, Wang H, Feng D, Tam J, Osei-Hyiaman D, Kunos G, Gao B. Biologically active, high levels of interleukin-22 inhibit hepatic gluconeogenesis but do not affect obesity and its metabolic consequences. *Cell Biosci* 2015;5:25.
 42. Zai W, Chen W, Wu Z, Jin X, Fan J, Zhang X, Luan J, Tang S, Mei X, Hao Q, Liu H, Ju D. Targeted interleukin-

- 22 gene delivery in the liver by polymetformin and penetration-based hybrid nanoparticles to treat nonalcoholic fatty liver disease. *ACS Appl Mater Interfaces* 2019;11:4842–4857.
43. Rolla S, Alchera E, Imarisio C, Bardina V, Valente G, Cappello P, Mombello C, Follenzi A, Novelli F, Carini R. The balance between IL-17 and IL-22 produced by liver-infiltrating T-helper cells critically controls NASH development in mice. *Clin Sci (Lond)* 2016; 130:193–203.
 44. Kriss M, Golden-Mason L, Kaplan J, Mirshahi F, Setiawan VW, Sanyal AJ, Rosen HR. Increased hepatic and circulating chemokine and osteopontin expression occurs early in human NAFLD development. *PLoS One* 2020;15:e0236353.
 45. Haas JT, Vonghia L, Mogilenko DA, Verrijken A, Molendic-Coste O, Fleury S, Deprince A, Nikitin A, Woitrain E, Ducrocq-Geoffroy L, Pic S, Derudas B, Dehondt H, Gheeraert C, Van Gaal L, Driessen A, Lefebvre P, Staels B, Francque S, Dombrowicz D. Author correction: transcriptional network analysis implicates altered hepatic immune function in NASH development and resolution. *Nat Metab* 2019;1:744.
 46. Zheng Y, Danilenko DM, Valdez P, Kasman I, Eastham-Anderson J, Wu J, Ouyang W. Interleukin-22, a T(H)17 cytokine, mediates IL-23-induced dermal inflammation and acanthosis. *Nature* 2007;445:648–651.
 47. Rensen SS, Slaats Y, Nijhuis J, Jans A, Bieghs V, Driessen A, Malle E, Greve JW, Buurman WA. Increased hepatic myeloperoxidase activity in obese subjects with nonalcoholic steatohepatitis. *Am J Pathol* 2009; 175:1473–1482.
 48. Itoh M, Kato H, Suganami T, Konuma K, Marumoto Y, Terai S, Sakugawa H, Kanai S, Hamaguchi M, Fukaishi T, Aoe S, Akiyoshi K, Komohara Y, Takeya M, Sakaida I, Ogawa Y. Hepatic crown-like structure: a unique histological feature in non-alcoholic steatohepatitis in mice and humans. *PLoS One* 2013;8:e82163.
 49. Krenkel O, Puengel T, Govaere O, Abdallah AT, Mossanen JC, Kohlhepp M, Liepelt A, Lefebvre E, Luedde T, Hellerbrand C, Weiskirchen R, Longerich T, Costa IG, Anstee QM, Trautwein C, Tacke F. Therapeutic inhibition of inflammatory monocyte recruitment reduces steatohepatitis and liver fibrosis. *Hepatology* 2018; 67:1270–1283.
 50. Cai B, Dongiovanni P, Corey KE, Wang X, Shmarakov IO, Zheng Z, Kasikara C, Davra V, Meroni M, Chung RT, Rothlin CV, Schwabe RF, Blaner WS, Birge RB, Valenti L, Tabas I. Macrophage MerTK promotes liver fibrosis in nonalcoholic steatohepatitis. *Cell Metab* 2020; 31:406–421.e7.
 51. Koop AC, Thiele ND, Steins D, Michaëlsson E, Wehmeyer M, Scheja L, Steglich B, Huber S, Schulze Zur Wiesch J, Lohse AW, Heeren J, Kluwe J. Therapeutic targeting of myeloperoxidase attenuates NASH in mice. *Hepatol Commun* 2020;4:1441–1458.
 52. Kisseleva T, Cong M, Paik Y, Scholten D, Jiang C, Benner C, Iwaisako K, Moore-Morris T, Scott B, Tsukamoto H, Evans SM, Dillmann W, Glass CK, Brenner DA. Myofibroblasts revert to an inactive phenotype during regression of liver fibrosis. *Proc Natl Acad Sci U S A* 2012;109:9448–9453.
 53. Hernandez-Gea V, Friedman SL. Pathogenesis of liver fibrosis. *Annu Rev Pathol* 2011;6:425–456.
 54. Feldstein AE, Canbay A, Angulo P, Taniai M, Burgart LJ, Lindor KD, Gores GJ. Hepatocyte apoptosis and fas expression are prominent features of human nonalcoholic steatohepatitis. *Gastroenterology* 2003;125:437–443.
 55. Thapaliya S, Wree A, Povero D, Inzaugarat ME, Berk M, Dixon L, Papouchado BG, Feldstein AE. Caspase 3 inactivation protects against hepatic cell death and ameliorates fibrogenesis in a diet-induced NASH model. *Dig Dis Sci* 2014;59:1197–1206.
 56. Støy S, Laursen TL, Glavind E, Eriksen PL, Terczynska-Dyla E, Magnusson NE, Hamilton-Dutoit S, Mortensen FV, Veidal SS, Rigbolt K, Riggio O, Deleuran B, Vilstrup H, Sandahl TD. Low interleukin-22 binding protein is associated with high mortality in alcoholic hepatitis and modulates interleukin-22 receptor expression. *Clin Transl Gastroenterol* 2020;11:e00197.
 57. Lee C, Kim J, Jung Y. Potential therapeutic application of estrogen in gender disparity of nonalcoholic fatty liver disease/nonalcoholic steatohepatitis. *Cells* 2019;8:1259.
 58. Kamada Y, Kiso S, Yoshida Y, Chatani N, Kizu T, Hamano M, Tsubakio M, Takemura T, Ezaki H, Hayashi N, Takehara T. Estrogen deficiency worsens steatohepatitis in mice fed high-fat and high-cholesterol diet. *Am J Physiol Gastrointest Liver Physiol* 2011; 301:G1031–G1043.
 59. Qi X, Yun C, Liao B, Qiao J, Pang Y. The therapeutic effect of interleukin-22 in high androgen-induced polycystic ovary syndrome. *J Endocrinol* 2020;245:281–289.
 60. Stülb H, Bachmann M, Gonther S, Mühl H. Acetaminophen-induced liver injury exposes murine IL-22 as sex-related gene product. *Int J Mol Sci* 2021;22:10623.
 61. Iwano R, Iwashita N, Takagi Y, Fukuyama T. Estrogen receptor α activation aggravates imiquimod-induced psoriasis-like dermatitis in mice by enhancing dendritic cell interleukin-23 secretion. *J Appl Toxicol* 2020;40:1353–1361.
 62. Stranges S, Dorn JM, Muti P, Freudenheim JL, Farinano E, Russell M, Nochajski TH, Trevisan M. Body fat distribution, relative weight, and liver enzyme levels: a population-based study. *Hepatology* 2004;39:754–763.
 63. Hamaguchi M, Okamura T, Fukuda T, Nishida K, Yoshimura Y, Hashimoto Y, Ushigome E, Nakanishi N, Majima S, Asano M, Yamazaki M, Takakuwa H, Kita M, Fukui M. Group 3 innate lymphoid cells protect steatohepatitis from high-fat diet induced toxicity. *Front Immunol* 2021;12:648754.
 64. Zheng Y, Valdez PA, Danilenko DM, Hu Y, Sa SM, Gong Q, Abbas AR, Modrusan Z, Ghilardi N, de Sauvage FJ, Ouyang W. Interleukin-22 mediates early host defense against attaching and effacing bacterial pathogens. *Nat Med* 2008;14:282–289.
 65. De Minicis S, Rychlicki C, Agostinelli L, Saccomanno S, Candelaresi C, Trozzi L, Mingarelli E, Facinelli B, Magi G, Palmieri C, Marziani M, Benedetti A, Svegliati-Baroni G. Dysbiosis contributes to fibrogenesis in the course of chronic liver injury in mice. *Hepatology* 2014; 59:1738–1749.

66. Loomba R, Seguritan V, Li W, Long T, Klitgord N, Bhatt A, Dulai PS, Caussy C, Bettencourt R, Highlander SK, Jones MB, Sirlin CB, Schnabl B, Brinkac L, Schork N, Chen CH, Brenner DA, Biggs W, Yooseph S, Venter JC, Nelson KE. Gut microbiome-based metagenomic signature for non-invasive detection of advanced fibrosis in human nonalcoholic fatty liver disease. *Cell Metab* 2017;25:1054–1062.e5.
67. Flores Molina M, Fabre T, Cleret-Buhot A, Soucy G, Meunier L, Abdelnabi MN, Belforte N, Turcotte S, Shoukry NH. Visualization, quantification, and mapping of immune cell populations in the tumor microenvironment. *J Vis Exp* 2020;157.
68. Jouihac H. Measurement of liver triglyceride content. *Bioprotocol* 2012;2:e223.

CRediT Authorship Contributions

Mohamed N Abdelnabi, MSc (Conceptualization: Lead; Data curation: Lead; Formal analysis: Lead; Investigation: Lead; Methodology: Lead; Writing – original draft: Lead)

Manuel Flores Molina, BSc (Data curation: Supporting; Investigation: Supporting; Writing – review & editing: Supporting)

Genevieve Soucy, MD (Formal analysis: Supporting)

Vincent Quoc-Huy Trinh, MD (Formal analysis: Supporting; Writing – review & editing: Supporting)

Nathalie Bedard, MSc (Investigation: Supporting; Resources: Supporting)

Sabrina Mazouz, MSc (Formal analysis: Supporting; Writing – review & editing: Supporting)

Nathalie Jouvét (Investigation: Supporting; Methodology: Supporting)

Jessica Dion, MSc (Investigation: Supporting)

Sarah Tran, MSc (Investigation: Supporting)

Marc Bilodeau, MD (Conceptualization: Supporting; Resources: Supporting)
Jennifer Estall (Conceptualization: Supporting; Writing – review & editing: Supporting)

Naglaa H. Shoukry, Ph.D. (Conceptualization: Lead; Funding acquisition: Lead; Supervision: Lead; Writing – original draft: Equal; Writing – review & editing: Lead)

Received February 18, 2022. Accepted August 8, 2022.

Correspondence

Address correspondence to: Naglaa H. Shoukry, PhD, Centre de Recherche du Centre Hospitalier de l'Université de Montréal, Tour Viger, Local R09.414, 900 Rue St-Denis, Montréal, Québec H2X 0A9, Canada. e-mail: Naglaa.shoukry@umontreal.ca; fax: (514) 412-7936.

Acknowledgments

The authors thank Dr Ghada S. Hassan for critical reading of the manuscript. The authors thank all study subjects for participating in this study and acknowledge the following CRCHUM platforms for excellent technical assistance: animal facility, molecular pathology, microscopy, flow cytometry, and rodent phenotyping-metabolic, cardiovascular, and cellular physiology service.

Conflicts of interest

The authors disclose no conflicts.

Funding

Supported by research grants from the Canadian Liver Foundation and the Canadian Institutes of Health Research (PJ4-169659 and PJT-175134); the Bourse d'Exemption des Droits de Scolarité Supplémentaires from the Université de Montréal and a doctoral fellowship from the Canadian Network on Hepatitis C (M.N.A.) (the Canadian Network on Hepatitis C is funded by a joint initiative of the Canadian Institutes of Health Research and the Public Health Agency of Canada grant HPC-178912); a doctoral fellowship from the Fonds de Recherche du Québec-Santé (M.F.M.); a doctoral fellowship from the Canadian Network on Hepatitis C (S.M.); and the Université de Montréal Novartis/Canadian Liver Foundation Hepatology Research Chair (M.B.). The study sponsors had no role in the study design or the collection, analysis, and interpretation of data.